

Self-assembly of hierarchically porous ZSM-5/SBA-16 with different morphologies and its high isomerization performance for hydrodesulfurization of dibenzothiophene and 4,6-dimethyldibenzothiophene

Xilong Wang, Jinlin Mei, Zhen Zhao, Peng Zheng, Zhentao Chen,
Daowei Gao, Jianye Fu, Jiyuan Fan, Aijun Duan, and Chunming Xu

ACS Catal., **Just Accepted Manuscript** • DOI: 10.1021/acscatal.7b04147 • Publication Date (Web): 19 Jan 2018

Downloaded from <http://pubs.acs.org> on January 19, 2018

Just Accepted

“Just Accepted” manuscripts have been peer-reviewed and accepted for publication. They are posted online prior to technical editing, formatting for publication and author proofing. The American Chemical Society provides “Just Accepted” as a free service to the research community to expedite the dissemination of scientific material as soon as possible after acceptance. “Just Accepted” manuscripts appear in full in PDF format accompanied by an HTML abstract. “Just Accepted” manuscripts have been fully peer reviewed, but should not be considered the official version of record. They are accessible to all readers and citable by the Digital Object Identifier (DOI®). “Just Accepted” is an optional service offered to authors. Therefore, the “Just Accepted” Web site may not include all articles that will be published in the journal. After a manuscript is technically edited and formatted, it will be removed from the “Just Accepted” Web site and published as an ASAP article. Note that technical editing may introduce minor changes to the manuscript text and/or graphics which could affect content, and all legal disclaimers and ethical guidelines that apply to the journal pertain. ACS cannot be held responsible for errors or consequences arising from the use of information contained in these “Just Accepted” manuscripts.



1
2
3
4 **Self-assembly of hierarchically porous ZSM-5/SBA-16 with**
5 **different morphologies and its high isomerization**
6 **performance for hydrodesulfurization of dibenzothiophene**
7 **and 4,6-dimethyldibenzothiophene**
8
9
10
11
12
13
14

15 Xilong Wang[†], Jinlin Mei[†], Zhen Zhao[†], Peng Zheng[†], Zhentao Chen[†], Daowei Gao
16
17
18 ‡, Jianye Fu[†], Jiyuan Fan[†], Aijun Duan^{*†}, Chunming Xu^{*†}
19
20
21
22
23

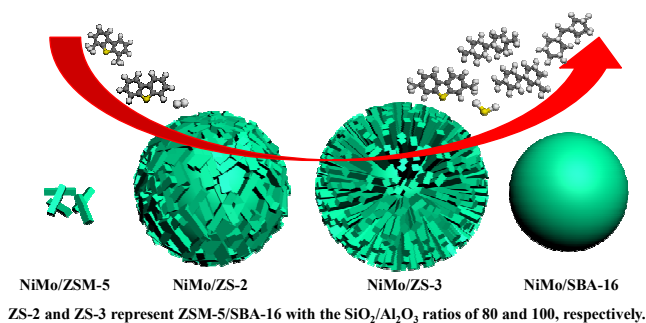
24 † *State Key Laboratory of Heavy Oil Processing, China University of Petroleum,*
25
26 *Beijing, 18 Fuxue Road, Beijing, P.R. China, 102249*
27
28

29 ‡ *School of Chemistry and Chemical Engineering, University of Jinan, Jinan, PR*
30
31 *China, 250022*
32
33
34
35
36

37
38 Corresponding Author: *E-mail: duanaijun@cup.edu.cn. Tel: +86 10 89732290.
39

40 *E-mail: xcm@cup.edu.cn. Tel: +86 10 89733392.
41
42
43
44
45
46
47
48
49
50
51
52
53
54
55
56
57
58
59
60

TOC graphic



Abstract

ZSM-5/SBA-16 (ZS) composite materials with different morphologies were synthesized successfully. The series supports were utilized to prepare the NiMo/ZS for the dibenzothiophene (DBT) and 4,6-dimethyldibenzothiophene (4,6-DMDBT) hydrodesulfurization (HDS) reactions. Series ZS supports and NiMo/ZS were well characterized to investigate their structure-property relationship. The NiMo/ZS catalyst (NiMo/ZS-3) with uniform morphology and well-ordered pore channels showed the maximum k_{HDS} and TOF values of DBT and 4,6-DMDBT HDS. The k_{HDS} ($13.9 \times 10^{-4} \text{ mol g}^{-1} \text{ h}^{-1}$) of DBT over NiMo/ZS-3 was more than two times as that over the reference NiMo/ZS-M catalyst ($5.5 \times 10^{-4} \text{ mol g}^{-1} \text{ h}^{-1}$), three times as that over the NiMo/SBA-16 catalyst ($4.4 \times 10^{-4} \text{ mol g}^{-1} \text{ h}^{-1}$), and almost four times as that over the NiMo/ZSM-5 catalyst ($3.5 \times 10^{-4} \text{ mol g}^{-1} \text{ h}^{-1}$). Furthermore, the k_{HDS} ($8.4 \times 10^{-4} \text{ mol g}^{-1} \text{ h}^{-1}$) of 4,6-DMDBT over NiMo/ZS-3 was more than three times as that over the reference NiMo/ZS-M catalyst ($2.8 \times 10^{-4} \text{ mol g}^{-1} \text{ h}^{-1}$), more than four times as that over the NiMo/SBA-16 catalyst ($1.7 \times 10^{-4} \text{ mol g}^{-1} \text{ h}^{-1}$) and almost five times as that over the NiMo/ZSM-5 catalyst ($1.6 \times 10^{-4} \text{ mol g}^{-1} \text{ h}^{-1}$). The superior DBT and

1
2
3 4,6-DMDBT HDS performance were assigned to the uniform morphology,
4 well-ordered pore channels, high B/L ratio of the NiMo/ZS-3 catalyst and the suitable
5 dispersion of the MoS₂ active phases. The HYD was the preferential route for DBT
6 HDS, while the ISO was the preferential route for 4,6-DMDBT HDS because of the
7 high B/L ratio of NiMo/ZS-3. Moreover, the DBT and 4,6-DMDBT HDS reaction
8 networks of the series NiMo/ZS were presented.
9
10
11
12
13
14
15
16
17
18

19 **Keywords**

20 ZSM-5/SBA-16; Morphology, Dibenzothiophene; 4,6-dimethyldibenzothiophene;
21 Hydrodesulfurization; Isomerization route
22
23
24
25
26
27

28 **1. INTRODUCTION**

29
30 Environmental pollution in many countries arised from undesirable toxic
31 emission from diesel engines has aroused public concern because of the high sulfur
32 content in diesel fuel.¹⁻⁴ Increasing strict environmental legislation in many countries
33 limits the sulfur content of diesel lower than 10 ppm.⁵⁻⁷ The great challenge in
34 producing the ultra-low-sulfur diesel is to eliminate the sulfur compounds with large
35 molecular weight, for instance, DBT and 4,6-DMDBT.⁸⁻¹² Nevertheless, complete
36 removal of 4,6-DMDBT over the conventional industrial catalysts (Ni-MoS₂/γ-Al₂O₃
37 and CoMoS₂/γ-Al₂O₃) is hard to achieve.¹³⁻¹⁶ In order to satisfy the increasing demand
38 for ultra-low-sulfur diesel, many methods have been studied, among which the
39 exploitation of more active support material is an economic way because the structure
40 of the sulfide active phase (orientation, morphology, size, sulfidation degree, etc) is
41
42
43
44
45
46
47
48
49
50
51
52
53
54
55
56
57
58
59
60

1
2
3 strongly influenced by the nature of the support itself.^{17, 18}
4
5

6 Zeolites, for instance, Y, ZSM-5, beta, mordenite and ferrierite, are important
7 candidates for petroleum industrial and environmental catalyst supports due to their
8 different shapes, sizes and connectivity of channels from 8 to 30 rings.¹⁹⁻²¹ Among
9 different zeolites, ZSM-5 is a versatile industrial catalyst due to its excellent
10 hydrogenation and isomerization performance.²²⁻²³ Sugioka et al.²⁴ reported that
11 Pt/HZSM-5 exhibited high and stable HDS catalytic activity of thiophene than that of
12 commercial CoMo/Al₂O₃ catalyst at 400 °C under 1 atm. Wu et al.²⁵ found that
13 nano-sized HZSM-5 synthesized hydrothermal crystallization method presented high
14 4,6-DMDBT isomerization performance, which could remove the steric hindrance of
15 alkyl-substitutes in the molecules of 4,6-DMDBT. However, the application of ZSM-5
16 in HDS process is limited because bulky sulfur compound molecules cannot diffuse
17 into the pore channels of ZSM-5.²⁶⁻²⁸
18
19
20
21
22
23
24
25
26
27
28
29
30
31
32
33
34

35 Mesoporous silica materials are of great interest for hydrodesulfurization (HDS)
36 catalyst supports because of its high specific surface areas and tunable pore
37 diameters.²⁹⁻³³ The superior structure properties facilitate mass transfer and high
38 dispersion of active phases. Valencia et al.³⁴ synthesized NiMo/SBA-15 modified
39 with citric acid and found that modified NiMo/SBA-15 displayed better HDS
40 performance compared with NiMo/SBA-15 without citric acid. Gao et al.³⁵ found that
41 NiMo/Al-SBA-15 with spherical morphology synthesized via hydrothermal synthesis
42 method exhibited high HDS activity with DBT conversion of 98.2% under 340 °C and
43 4.0 MPa. However, these two-dimensional hexagonal materials cannot provide more
44
45
46
47
48
49
50
51
52
53
54
55
56
57
58
59
60

1
2
3 favorable mass transfer for reactant and product molecules.³⁶ SBA-16 material
4 exhibits three-dimensional cubic arrangement (Im3m) of mesopores and each
5
6 nanocage pore in SBA-16 is interconnected to eight neighboring cages through pore
7
8 entrance, which are in favor of the effective transport of reactant and product
9
10 molecules.^{37, 38} However, pure mesoporous silica materials have no B and L sites,
11
12 which are detrimental to the hydrogenation and isomerization performance for HDS
13
14 reaction.³⁹ Moreover, the amorphous structure of pure mesoporous silica materials
15
16 indicates that the thermal and hydrothermal stabilities of mesoporous silica are
17
18 inherently lower than those of zeolites.
19
20
21
22
23
24

25
26 It is well known that hydrogen spillover can vastly facilitate the hydrogenation
27
28 ability, which could induce to the great improvement of the HDS activity.^{40, 41} Tang et
29
30 al.⁴² synthesized the bunchy mordenite nanofibers and found that the spillover
31
32 hydrogen generated in micropores could transfer to the nearby active phases in the
33
34 mesopores. To overcome the limitations of individual zeolites and mesoporous
35
36 materials in the HDS reactions, the design of hierarchically porous composites
37
38 combining the superiority of zeolites and mesoporous materials is very important.
39
40 Lots of micro-mesoporous composites, for instance, Beta-MCM-41⁴³ and
41
42 Beta-SBA-15⁴⁴, were prepared and used in the catalysis. Certainly, our research
43
44 group has a good research foundation for the synthesis of micro-mesoporous
45
46 composite material. There were previous work in our research group on the
47
48 hierarchically porous material and the application of the composite material in HDS
49
50 reaction. Zhang et al.³⁹ found that NiMo/Beta-KIT-6 showed much better DBT HDS
51
52
53
54
55
56
57
58
59
60

1
2
3 activities than the commercial NiMo/ γ -Al₂O₃ catalyst. Wu et al.²⁵ found that
4
5 NiMo/ZSM-5-KIT-6 catalyst showed the superior isomerization selectivity of
6
7 4,6-DMDBT HDS. Through these previous researches we found that the synergistic
8
9 effect between microporous and mesoporous phases could vastly facilitate the HDS
10
11 activity. However, the phases of microporous phase and mesoporous phase in the
12
13 previous researches were separated. And the synergistic effect between microporous
14
15 and mesoporous phases was not utilized well. It was difficult to synthesize
16
17 homogeneous composites with uniform morphologies and it was also difficult to
18
19 prove the successful synthesis of homogeneous composites. Based on the
20
21 imperfection and the difficulties of the synthesis of the micro-mesoporous composite
22
23 material, the exploration of the synthesis methods of homogeneous composite
24
25 materials with uniform morphologies was necessary. The phases and the
26
27 morphologies of homogeneous composite materials were controlled by the
28
29 precipitation rate of the silicon sources and the hydrolysis rate of the organic
30
31 templates.
32
33
34
35
36
37
38
39

40 In this research, ZS composite materials with different uniform morphologies
41
42 were synthesized from ZSM-5 seeds by modulating silicon source, inorganic salts
43
44 (Figure S1 in Supporting Information), aging temperatures (Figure S2 in Supporting
45
46 Information), the concentrations of HCl (Figure S3 in Supporting Information), and
47
48 SiO₂/Al₂O₃ ratios (60/80/100/120/140). It was also proved indirectly that partial Al
49
50 species attributed to ZSM-5 were introduced into the SBA-16 framework, indicating
51
52 the successful synthesis of ZSM-5/SBA-16 composites. Series NiMo/ZS catalysts
53
54
55
56
57
58
59
60

1
2
3 were evaluated in the DBT and 4,6-DMDBT HDS. Moreover, to study the influences
4 of pore channels and acidic sites on DBT and 4,6-DMDBT HDS performance,
5 different supports such as ZSM-5 zeolite, SBA-16, ZSM-5 seeds and SBA-16 mixture
6 (ZS-M), were selected as the reference supports. The NiMo/ZS exhibited better DBT
7 and 4,6-DMDBT HDS performance. HYD and ISO were the prior routes of the DBT
8 and 4,6-DMDBT HDS, respectively, which were because of the higher of B/L ratio of
9 the NiMo/ZS catalyst. Moreover, the DBT and 4,6-DMDBT HDS reaction network of
10 series NiMo/ZS were presented.
11
12
13
14
15
16
17
18
19
20
21
22
23
24

25 **2. EXPERIMENTAL SECTION**

26 **2.1 Synthesis of the supports and catalysts**

27 **2.1.1 Synthesis of ZSM-5 seed**

28
29
30
31
32 ZSM-5 seed ($\text{SiO}_2/\text{Al}_2\text{O}_3$ molar ratio = 30) was prepared from the mixture of
33 $\text{SiO}_2/\text{Al}_2\text{O}_3/\text{TPABr}/\text{NaOH}/\text{H}_2\text{O}$ with a molar ratio of 30/1.0/5.0/21/450. 0.287 g
34 NaOH, 1.0 g NaAlO_2 (45 wt% Al_2O_3) and 20 g H_2O were stirred together for 1.0 h at
35 25 °C (denoted as Solution A). 0.6 g NaOH, 5.3 g TPABr and 16 g H_2O were stirred
36 together for 15 min (denoted as Solution B), then 20 g of colloidal silica (40 wt%
37 SiO_2) was poured into solution B dropwise and stirred rapidly for 1.0 h at 25 °C
38 (denoted as Solution C). Solution A was added into Solution C dropwise and stirred
39 rapidly for 3.0 h at 25 °C. Afterwards, the homogenous gel was put into an autoclave
40 and crystallized at 170 °C for 32 h to obtain zeolite ZSM-5 seed solution. All details
41 of the reagents were listed in Table S1 (in Supporting Information).
42
43
44
45
46
47
48
49
50
51
52
53
54
55
56
57
58
59
60

2.1.2 Synthesis of ZS materials

ZS composites were synthesized using EO₁₀₆PO₇₀EO₁₀₆ (F127) as the template and tetraethylorthosilicate (TEOS) as the silica source. 4.0 g of F127, 10 g of KCl and 240 mL of HCl (1.5 mol/L) were stirred together for 2.0 h at 35 °C. 12.0 g of cosurfactant butanol was added into the mixed solutions and stirred rapidly for 2.0 h at 35 °C. Then 16.6 g of TEOS (28.4 wt.% SiO₂) was added into the mixtures dropwise and stirred for 30 min, after that, different amounts of zeolite ZSM-5 seed (37.14, 22.29, 15.92, 12.38 and 10.12 g, respectively) were added into these mixtures and stirred for 1.0 h, subsequently, kept motionless for 24 h before putting into five autoclaves and maintained at 100 °C for 24 h. The solids were obtained by filtration, dried at 90 °C for 8.0 h, and calcined at 550 °C for 6.0 h. The ZS materials with different molar ratios of SiO₂/Al₂O₃ (60, 80, 100, 120 and 140) synthesized with different amounts of zeolite ZSM-5 seed (37.14, 22.29, 15.92, 12.38 and 10.12 g) were denoted as ZS-1, ZS-2, ZS-3, ZS-4 and ZS-5, correspondingly. The preparation scheme of ZSM-5/SBA-16 composites with various morphologies was displayed in Scheme S1 (in Supporting Information).

2.1.3 Synthesis of the reference materials

For comparison, reference materials (ZSM-5, SBA-16 and ZS-M) were synthesized. ZSM-5 with higher crystalline degree was obtained at the crystallization time of 72 h. Mesoporous SBA-16 material was prepared using the same method with

1
2
3 ZS material without the addition of ZSM-5 seed. ZS-M material was the mixture of
4
5 ZSM-5 seed and SBA-16 with a molar ratio of $\text{SiO}_2/\text{Al}_2\text{O}_3 = 100$.
6
7
8
9

10 **2.1.4 Synthesis of the corresponding catalysts**

11
12 Prior to the preparation of catalysts, ZS series materials, ZSM-5 and ZS-M were
13
14 pretreated twice by ion exchange using ammonium chloride solution at 90 °C for 2.0 h.
15
16 All of the corresponding NiMo catalysts contained 15.0 wt% MoO_3 and 3.5 wt% NiO
17
18 were prepared as described in our previous work.⁴⁵ The corresponding NiMo catalysts
19
20 were recorded as NiMo/ZSM-5, NiMo/SBA-16, NiMo/ZS-M, NiMo/ZS-1,
21
22 NiMo/ZS-2, NiMo/ZS-3, NiMo/ZS-4 and NiMo/ZS-5, respectively.
23
24
25
26
27

28 **2.2 Characterization of the supports and the catalysts**

29
30
31 The detailed descriptions of different characterization methods, for instance,
32
33 X-ray diffraction (XRD), Nitrogen physisorptions, Scanning electron microscopy
34
35 (SEM), Transmission electron microscopy (TEM), Pyridine-FTIR, Raman spectra,
36
37 X-ray photoelectron spectra (XPS), High-resolution transmission electron microscopy
38
39 (HRTEM) and gas chromatography-mass spectrometry (GC-MS), were provided in
40
41 our previous work^{45,46}. ²⁷Al nuclear magnetic resonance (²⁷Al NMR) measurements
42
43 of series supports were performed on a Bruker Avance III 500 MHz spectrometer.
44
45
46
47
48
49

50 **2.3 Evaluation of HDS performance of catalysts**

51
52
53 The HDS catalytic activities were carried out by using DBT or 4,6-DMDBT as
54
55 reactants in a fix-bed reactor. Before reaction, all the fresh catalysts were presulfided
56
57

1
2
3 using 2.5 wt% CS₂ in cyclohexane solution at 340 °C, 4.0 MPa, 600 mL mL⁻¹, and 8.0
4
5 h⁻¹ for 4 h. Liquid feeds, DBT (500 ppm sulfur contents) dissolved in cyclohexane or
6
7 4,6-DMDBT (500 ppm sulfur contents) dissolved in toluene, were fed into the reactor
8
9 by a 5963 Optos 1LM 3/32 Head Eldex pump. The catalysts were tested at 340 °C, 4.0
10
11 MPa, 200 mL mL⁻¹, and different WHSVs of 10-100 h⁻¹.
12
13
14
15

16 The sulfur contents of feedstock and resulting products were measured using a
17
18 RPP-2000SN analyzer. The DBT or 4,6-DMDBT HDS conversion (%) was calculated
19
20 from Equation (3):
21
22

$$23 \quad HDS (\%) = (S_f - S_p) / S_f \times 100\% \quad (3)$$

24 where S_f is the sulfur content (ppm) of the feeds and S_p the sulfur content (ppm)
25
26 of the products.
27
28
29

30 Figures S4 (in Supporting Information) displayed the DBT and 4,6-DMDBT
31
32 HDS conversions of three catalysts (NiMo/ZS-3, NiMo/ZSM-5 and NiMo/SBA-16)
33
34 with different particle sizes (40-60 mesh). In this DBT and 4,6-DMDBT HDS
35
36 reaction systems, at the DBT and 4,6-DMDBT HDS conversions of about 50%, the
37
38 influence of mass transfer could be ruled out. The calculation method of k_{HDS} ,
39
40 Turn-over frequency (TOF , h⁻¹) and f_{Mo} were described in the previous published
41
42 researches.^{47, 48, 49}
43
44
45
46
47
48
49

50 **3. RESULTS**

51 **3.1 Characterization of the supports**

52 **3.1.1 XRD of the supports**

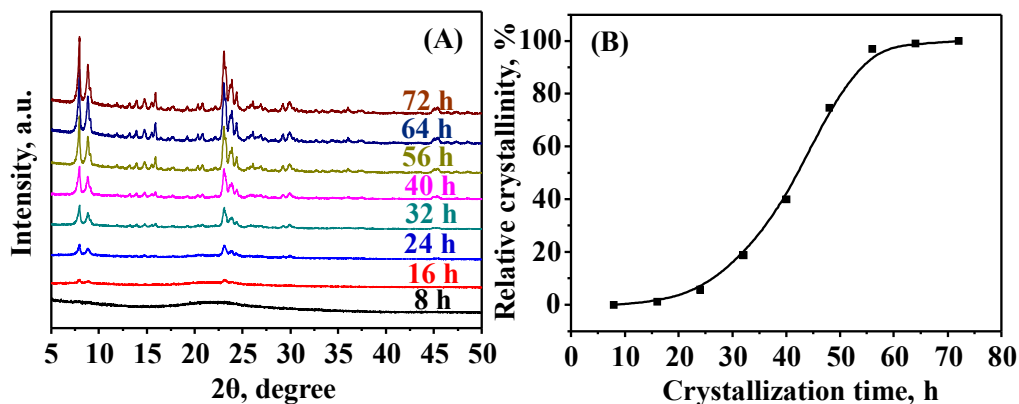


Figure 1. (A) Wide angle XRD and (B) relative crystallinity of ZSM-5 obtained by different crystallization times.

To assess the degree of crystallinity and control the particle size of ZSM-5 seeds, the ZSM-5 seeds were obtained by different crystallization times (between 8 h and 72 h) at 170 °C. The wide-angle XRD patterns and relative crystallinity curve of ZSM-5 seeds obtained under different crystallization times are shown in Figure 1. The as-synthesized ZSM-5 seeds show intense XRD peaks at $2\theta = 7.9^\circ, 8.8^\circ, 20.3^\circ, 23.1^\circ, 23.9^\circ$ and 29.9° corresponding well to the (101), (200), (103), (501), (303) and (503) planes of ZSM-5.⁵⁰ As the crystallization time increases to 24 h, the diffraction peaks assigned to ZSM-5 crystal are detected, suggesting that the nanocrystalline units of the ZSM-5 crystals are beginning to form. ZSM-5 seed obtained by the crystallization time of 32 h possesses more nanocrystalline units and appropriate particle sizes, which is in favor of synthesizing ZS micro-mesoporous composite materials. As the crystallization time increases to 72 h, the diffraction peak intensities attributed to ZSM-5 crystal are relatively strong, suggesting the crystallinity degree of the ZSM-5 crystals is relatively high, which can be used as the reference Zeolite ZSM-5 material.

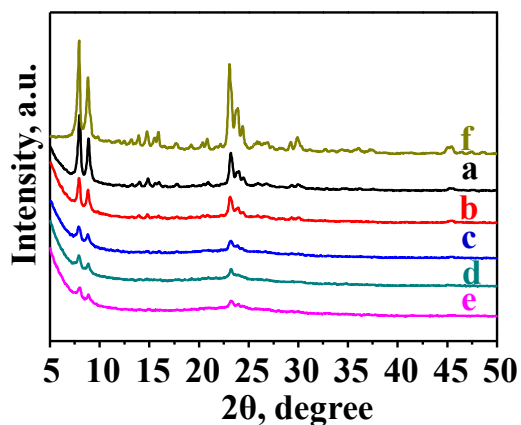


Figure 2. Wide angle XRD of ZS series composites and ZSM-5. (a) ZS-1, (b) ZS-2, (c) ZS-3, (d) ZS-4, (e) ZS-5, (f) ZSM-5.

As shown in Figure 2, all the series ZS materials and ZSM-5 obtained at the crystallization time of 72 h exhibit six peaks corresponding to the planes of ZSM-5. The peak intensities change in the sequence of ZSM-5 > ZS-1 > ZS-2 > ZS-3 > ZS-4 > ZS-5, indicating that the amounts of the nanocrystalline units follow the same order.

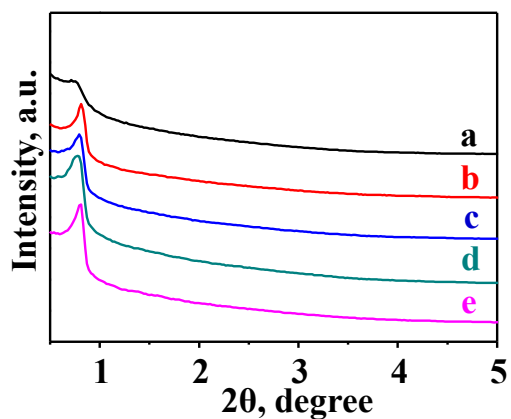
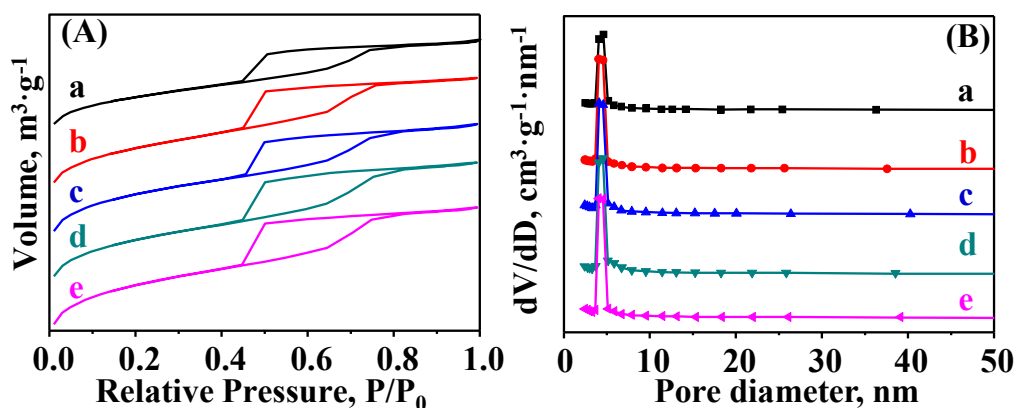


Figure 3. Small angle XRD of ZS series composites. (a) ZS-1, (b) ZS-2, (c) ZS-3, (d) ZS-4, (e) ZS-5.

1
2
3
4 The small angle XRD patterns of ZS series materials are displayed in Figure 3.
5
6 All the samples show characteristic peaks at the region of $2\theta = 0.8-1.5^\circ$,
7
8 corresponding to SBA-16 with 3D cubic ($Im\bar{3}m$) mesostructure.⁵¹ The characteristic
9
10 peaks also have these trends to become narrower and higher with the decrease of the
11
12 ZSM-5 seed contents, manifesting that the degrees of order increase.

17 3.1.2 N₂ physisorption of the supports

19 The N₂ physisorption isotherms and the pore size distribution of series ZS are
20
21 exhibited on Figures 4 (A) and (B). As shown in Figure 4 (A), the physisorption
22
23 isotherms of the ZS series supports exhibit type-IV curves, demonstrating that all the
24
25 ZS supports possess mesoporous structure. The pore size distributions of the series ZS
26
27 supports show relatively narrow distributions of mesopores and the concentration
28
29 degree of the series ZS supports change in sequence of $ZS-1 < ZS-2 < ZS-3 < ZS-4 <$
30
31 $ZS-5$, which are well consistent with the small angle XRD results.



52 **Figure 4.** (A) physisorption isotherms and (B) pore size distribution patterns of series ZS.

53 (a) ZS-1, (b) ZS-2, (c) ZS-3, (d) ZS-4, (e) ZS-5.

The corresponding properties of the series ZS supports are shown in Table S2 (in Supporting Information). The BET surface area, pore size and volume of series ZS change in sequence of ZS-1 ($647.42 \text{ m}^2 \text{ g}^{-1}$, 4.16 nm , $0.41 \text{ cm}^3 \text{ g}^{-1}$) < ZS-2 ($747.61 \text{ m}^2 \text{ g}^{-1}$, 4.19 nm , $0.51 \text{ cm}^3 \text{ g}^{-1}$) < ZS-3 ($751.96 \text{ m}^2 \text{ g}^{-1}$, 4.23 nm , $0.52 \text{ cm}^3 \text{ g}^{-1}$) < ZS-4 ($768.21 \text{ m}^2 \text{ g}^{-1}$, 4.30 nm , $0.54 \text{ cm}^3 \text{ g}^{-1}$) < ZS-5 ($792.62 \text{ m}^2 \text{ g}^{-1}$, 4.31 nm , $0.56 \text{ cm}^3 \text{ g}^{-1}$) < SBA-16 ($842.16 \text{ m}^2 \text{ g}^{-1}$, 4.05 nm , $0.66 \text{ cm}^3 \text{ g}^{-1}$).

3.1.3 ^{27}Al MAS NMR of the supports

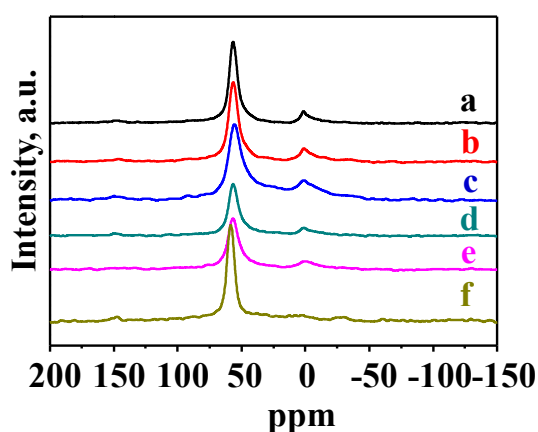


Figure 5. ^{27}Al MAS NMR spectra of the series ZS supports. (a) ZS-1, (b) ZS-2, (c) ZS-3, (d) ZS-4, (e) ZS-5, (f) ZSM-5.

The coordination information of Al atoms in the ZS series supports can be obtained from ^{27}Al MAS NMR. Figure 5 displays the ^{27}Al MAS NMR spectra of series ZS and ZSM-5 zeolite. Two signals at 0 and 54 ppm are assigned to the octahedral (extra-framework Al species) and tetrahedral coordinated aluminum atoms, respectively.⁵² The framework/extra-framework Al ratios in the series ZS and ZSM-5 supports follow the order of ZSM-5 > ZS-3 > ZS-2 > ZS-1 > ZS-4 > ZS-5. The ^{27}Al MAS NMR spectra (Figure S7, in Supporting Information) indicate that partial Al atoms were incorporated into the framework of the silica SBA-16 materials.

3.1.4 TEM images of the supports

The TEM images of the series ZS and pure SBA-16 materials are exhibited in Figure S5 (in Supporting Information). The series ZS and pure SBA-16 supports display well-ordered arrays of mesopores, revealing that they all have cubic body-centred $Im\bar{3}m$ symmetry structure. The mesoporous structures are partially destroyed with the increase of the ZSM-5 seed contents. It is hard to distinguish directly the MFI topology structure of ZSM-5, while we can get some information indirectly from the HAADF-STEM & EDX elemental mapping images (Figure S9). The Al mapping image of ZS-3 material shows that the Al atoms is uniformly dispersed in ZSM-5/SBA-16 composite material, demonstrating that the primary and secondary structures of ZSM-5 construct ZSM-5/SBA-16.

3.1.5 SEM images of the supports

The morphologies of the ZS series, ZSM-5, pure SBA-16 and ZS-M are studied by using SEM and the images of these supports are displayed in Figure 6. As shown in Figure 6 (a), the ZSM-5 phase is present in the form of partial hexagonal prism mono-crystals. The pure SBA-16 phase (Figure 6 (b)) is present in the form of uniform spherical aggregates with the sizes ranging from 7 to 9 μm . For the mechanical mixture of the pure SBA-16 and ZSM-5 seed, Figure 6 (h) clearly shows two separated phases, of which the uniform spherical aggregates are ascribed to SBA-16 and the small particles are ZSM-5 seeds. Figure 6 (c) and (g) show that the tenacity of each aggregate decreases with the decreasing content of the ZSM-5 seed in the composite, while the regularity of the spherical aggregates increases with the

1
2
3 decreasing content of the ZSM-5 seed. ZS-3 composite material is present in the form
4
5 of uniform spherical aggregates with the sizes ranging from 14 to 15 μm consisting of
6
7 uniform hexagonal prism mono-crystals, which presents an absolutely different
8
9 morphology from that of ZS-M. The pH value of the media varies during the addition
10
11 of different amounts of ZSM-5 seeds. The precipitation rate of the silicate species and
12
13 the hydrolysis rate of the surfactant are influenced greatly by the acid concentration.
14
15 Therefore, using different acidic concentrations and butanol additives modulate the
16
17 condensation rate of the inorganic chemicals, yielding different morphologies of the
18
19 ZS series supports.
20
21

22 Combined with the ^{27}Al MAS NMR spectra (Figure S7, in Supporting
23
24 Information), Al 2p XPS results (Figure S8, in Supporting Information) and
25
26 HAADF-STEM & EDX elemental mapping images (Figure S9, in Supporting
27
28 Information), it could be deduced that parts of ZSM-5 seeds were embedded in the
29
30 external surface and most of ZSM-5 seeds with small particle sizes were incorporated
31
32 into the wall of ZS-3 composite material via the Al-O-Si covalent bonding.
33
34
35
36
37
38
39
40
41
42
43
44
45
46
47
48
49
50
51
52
53
54
55
56
57
58
59
60

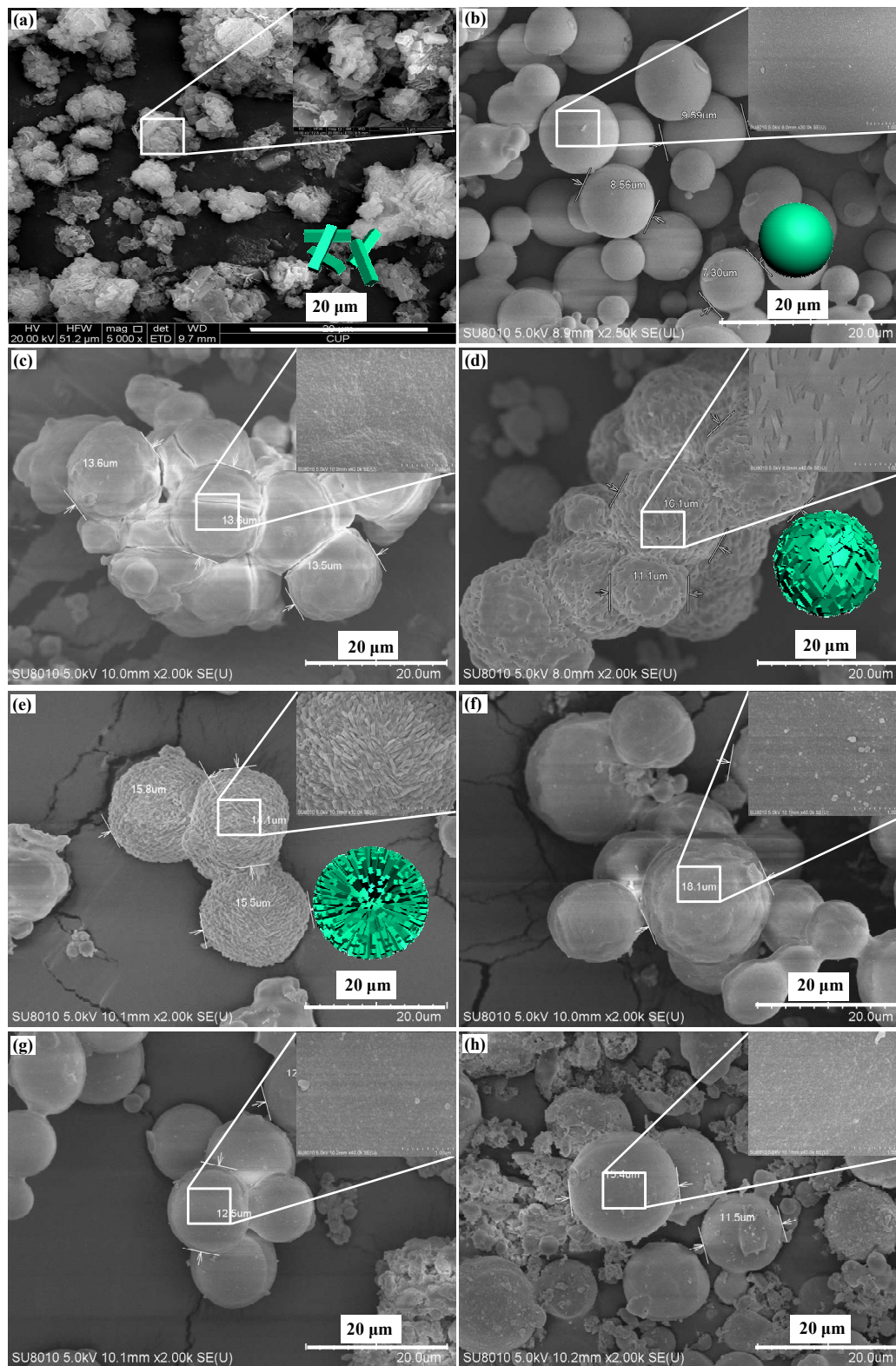


Figure 6. SEM images of the series ZS and pure SBA-16 supports. (a) ZSM-5, (b) SBA-16, (c) ZS-1, (d) ZS-2, (e) ZS-3, (f) ZS-4, (g) ZS-5, (h) ZS-M.

3.2 Characterization of the catalysts

3.2.1 Pyridine-FTIR of the oxide catalysts

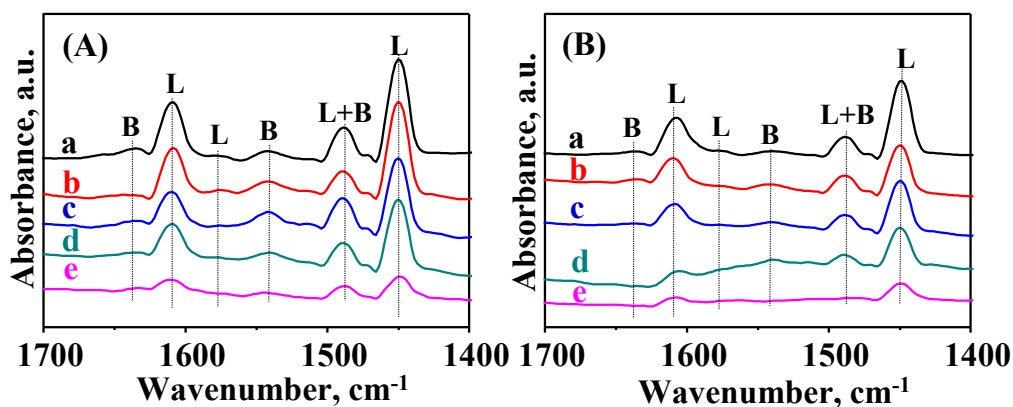


Figure 7. FTIR-pyridine spectra of different catalysts (a) NiMo/ZS-1, (b) NiMo/ZS-2, (c) NiMo/ZS-3, (d) NiMo/ZS-4 and (e) NiMo/ZS-5 after degassing at (A) 200 °C and (B) 350 °C.

Pyridine-FTIR spectroscopies of the series NiMo/ZS were recorded to investigate the acidic strength and types. The IR adsorption spectra of pyridine molecules (degas at 200 °C) are ascribed to the total acid amounts of the series catalysts, and the IR adsorption spectra of pyridine molecules (degas at 350 °C) are ascribed to the medium and strong acid amounts. Figure 7 shows the pyridine-FTIR adsorption spectra of series NiMo/ZS. The peaks at 1446, 1492, 1575 and 1622 cm^{-1} are assigned to L acid and the peaks at 1546 and 1639 cm^{-1} are assigned to B acid.³⁹ The peak intensities increase in the following order: NiMo/ZS-1 > NiMo/ZS-2 > NiMo/ZS-3 > NiMo/ZS-4 > NiMo/ZS-5.

The acid amounts of the NiMo/ZS are summarized in Table S3 (in Supporting Information). The total acid, the medium and strong acid amounts all increase with the following order: NiMo/ZS-1 (208 $\mu\text{mol g}^{-1}$, 133 $\mu\text{mol g}^{-1}$) > NiMo/ZS-2 (192

1
2
3 $\mu\text{mol g}^{-1}$, $91 \mu\text{mol g}^{-1}$) > NiMo/ZS-3 ($165 \mu\text{mol g}^{-1}$, $65 \mu\text{mol g}^{-1}$) > NiMo/ZS-4 (145
4 $\mu\text{mol g}^{-1}$, $50 \mu\text{mol g}^{-1}$) > NiMo/ZS-5 ($131 \mu\text{mol g}^{-1}$, $26 \mu\text{mol g}^{-1}$). The B/L ratios of the
5
6 total acid, and the medium and strong acid follow the order of NiMo/ZS-3 (0.23,
7
8 0.25) > NiMo/ZS-2 (0.21, 0.21) > NiMo/ZS-1 (0.20, 0.20) > NiMo/ZS-4 (0.17,
9
10 0.19) > NiMo/ZS-5 (0.14, 0.18), which is in accordance with the ^{27}Al MAS NMR
11
12 results, indicating that the incorporation of the Al atoms into SBA-16 framework
13
14 favors the improvement of B acid.
15
16
17
18
19
20

21 **3.2.2 H₂-TPR of the oxide catalysts**

22
23
24 H_2 -TPR of series NiMo/ZS was recorded to investigate the metal-support
25
26 interaction (MSI) and the reducibility of the oxide phases, the results are displayed in
27
28 Figure 8. The series NiMo/ZS show the low-temperature characteristic peaks due to
29
30 the reduction of polymeric octahedral coordination Mo species
31
32 ($\text{Mo}^{6+} \rightarrow \text{HxMoO}_3 \rightarrow \text{Mo}^{4+}$) at the range of 400-600 °C and high-temperature
33
34 characteristic peaks due to the deep reduction ($\text{Mo}^{4+} + 2\text{e}^- \rightarrow \text{Mo}^0$) of tetrahedrally
35
36 coordinated monomeric Mo species at the range of 700-900 °C.⁵³ The first reduction
37
38 temperatures and the deep reduction temperatures all follow the order of NiMo/ZS-1
39
40 (534 °C, 832 °C) > NiMo/ZS-2 (520 °C, 824 °C) > NiMo/ZS-3 (512 °C, 817 °C) >
41
42 NiMo/ZS-4 (505 °C, 812 °C) > NiMo/ZS-5 (499 °C, 792 °C), demonstrating that the
43
44 MSIs of series NiMo/ZS change in the identical rule. The NiMo/ZS-3 catalyst not
45
46 only has much weaker MSI than NiMo/ZS-1 and NiMo/ZS-2 catalysts, but also
47
48 obtains suitable dispersion of active Mo species than NiMo/ZS-4 and NiMo/ZS-5
49
50 catalysts.
51
52
53
54
55
56
57
58
59
60

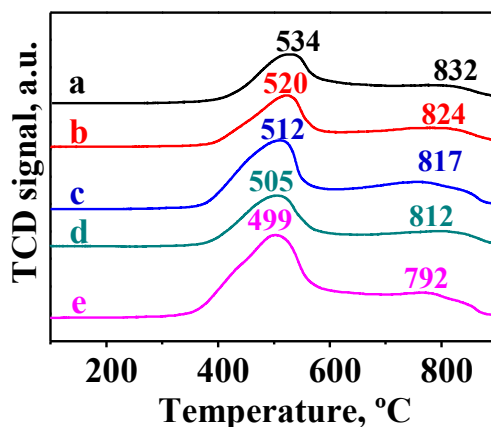


Figure 8. H₂-TPR of various oxide catalysts. (a) NiMo/ZS-1, (b) NiMo/ZS-2, (c) NiMo/ZS-3, (d) NiMo/ZS-4 and (e) NiMo/ZS-5.

3.2.3 Raman of the oxide and sulfide catalysts

Figure 9 displays the Raman spectra of the NiMo/ZS series oxide and sulfide catalysts. Figure 9 (A) shows that the Raman spectra of the series oxide catalysts have three peaks at 826, 908 and 955 cm⁻¹ assigned to the NiMoO₄ phase⁵⁴, a peak at 331 cm⁻¹ attributed to the terminal Mo=O bending mode of octahedral MoO₄²⁻ species, and a peak at 564 cm⁻¹ assigned to Al-O stretching mode.^{55, 56} Especially, the broad peak at 890-1000cm⁻¹ are characteristic of M=O stretching vibrations, indicating a weak MSI.⁵⁷ The peak intensities at 890-1000 cm⁻¹ follow the order of NiMo/ZS-5 > NiMo/ZS-4 > NiMo/ZS-3 > NiMo/ZS-2 > NiMo/ZS-1, which demonstrates that the MSIs decrease in the inverse order. The result agrees well with the H₂-TPR characterization. Figure 9 (B) displays the Raman spectra of the series sulfide catalysts have two peaks at 380 and 405 cm⁻¹ attributed to E_{2g}¹ and A_{1g} of MoS₂

crystalline structures and two peaks at 454 and 634 cm^{-1} are ascribed to the resonance scattering.^{58, 59} The intensities of the bands follow the order of NiMo/ZS-3 > NiMo/ZS-2 > NiMo/ZS-1 > NiMo/ZS-4 > NiMo/ZS-5, demonstrating that the sulfidation degree of the active phases changes in the same rule. The Raman spectra of the NiMo/ZS series oxide and sulfide catalysts show that the majority of oxide Mo species are sulfided to MoS₂ phases after the presulfurization treatment.

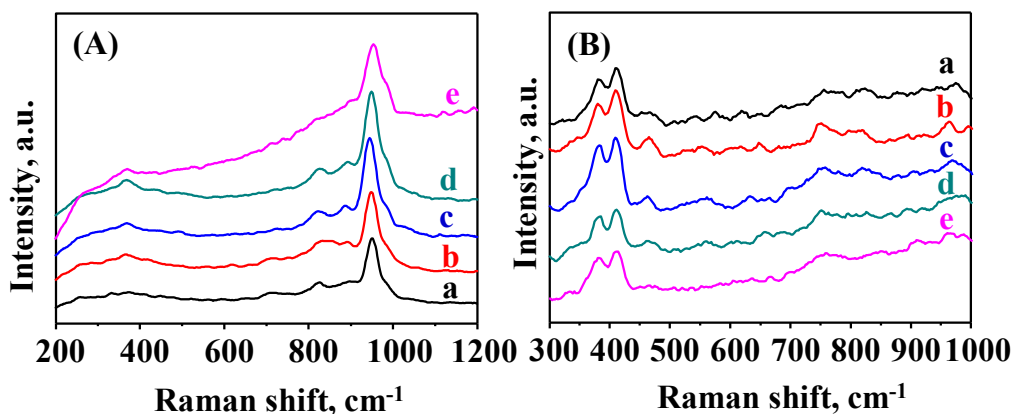


Figure 9. Raman spectra of (A) oxide catalysts and (B) sulfided catalysts. (a) NiMo/ZS-1, (b) NiMo/ZS-2, (c) NiMo/ZS-3, (d) NiMo/ZS-4 and (e) NiMo/ZS-5.

3.2.4 XPS of the sulfide catalysts

The surface composition and chemical state of the series NiMo/ZS and NiMo/ZS-M sulfide catalysts were recorded by XPS characterizations and the Mo3d XPS deconvolution results of the NiMo/ZS and NiMo/ZS-M series sulfide catalysts are shown in Figure 10. The standards for the fitting are described in our previous work.⁴⁵ The related Mo3d XPS results of series sulfide catalysts are listed in Table S4 (in Supporting Information). The sulfidation degrees change in the sequence of

NiMo/ZS-3 (69 %) > NiMo/ZS-2 (63 %) > NiMo/ZS-1 (56 %) > NiMo/ZS-4 (54 %) > NiMo/ZS-5 (52 %) > NiMo/ZS-M (49 %), which is in well accordance with the Raman results of the corresponding sulfide catalysts.

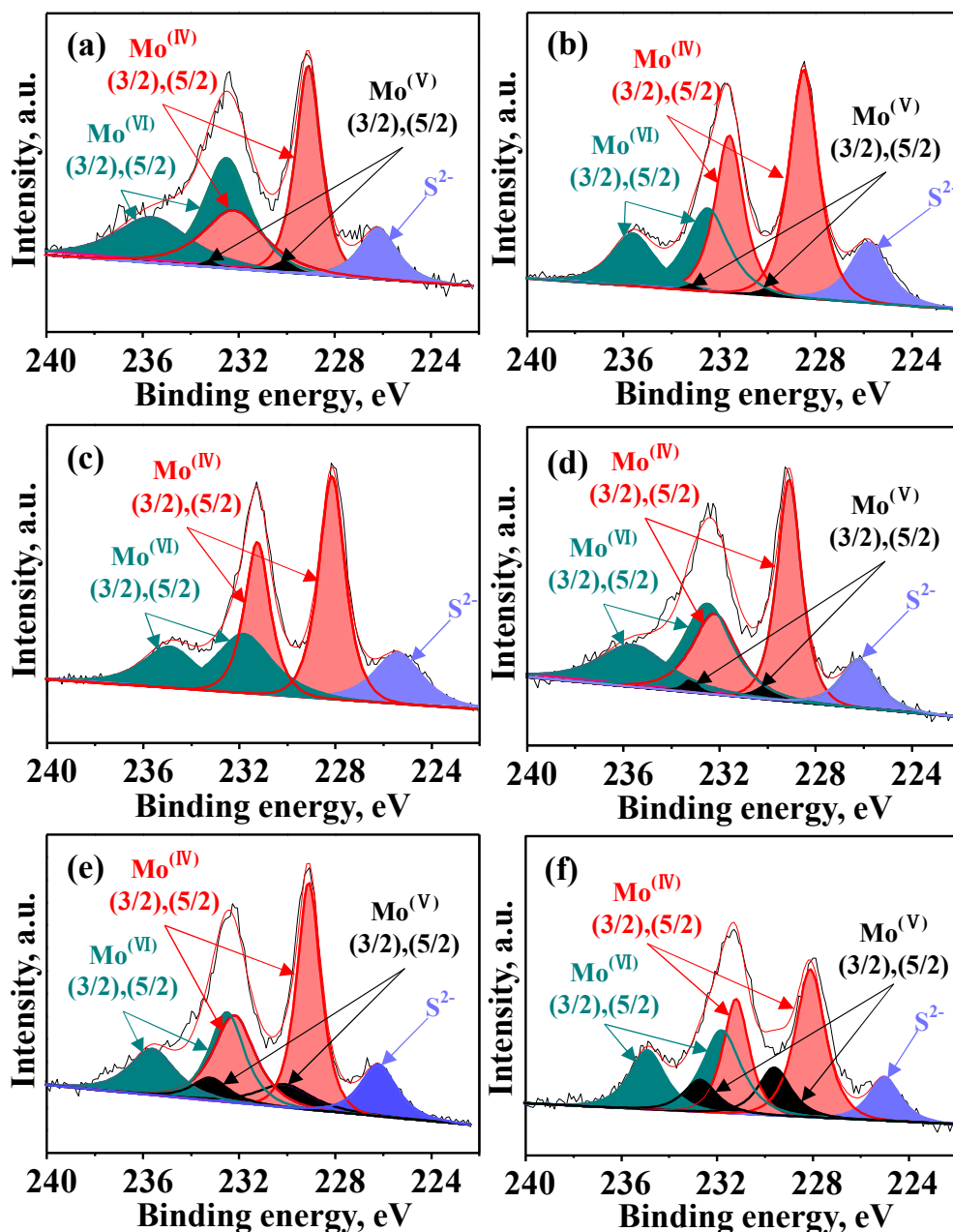


Figure 10. Mo3d XPS spectra of various sulfided catalysts. (a) NiMo/ZS-1, (b) NiMo/ZS-2, (c) NiMo/ZS-3, (d) NiMo/ZS-4, (e) NiMo/ZS-5 and (f) NiMo/ZS-M.

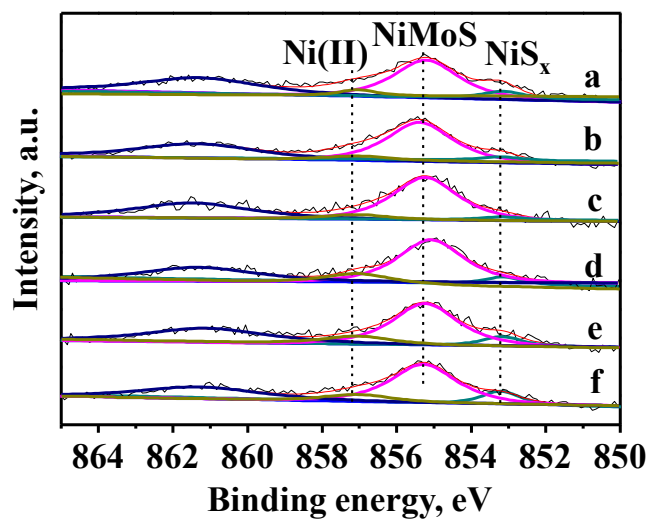


Figure 11. Ni_{2p} XPS spectra of the sulfided catalysts. (a) NiMo/ZS-1, (b) NiMo/ZS-2, (c) NiMo/ZS-3, (d) NiMo/ZS-4, (e) NiMo/ZS-5 and (f) NiMo/ZS-M.

The Ni_{2p} XPS spectra of series NiMo/ZS and NiMo/ZS-M sulfide catalysts are displayed in Figure 11 and the Ni_{2p} XPS deconvolution results of the NiMo/ZS and NiMo/ZS-M series sulfide catalysts are listed in Table S5 (in Supporting Information). The NiMoS ratios of the NiMo/ZS and NiMo/ZS-M series sulfide catalysts follow the order of NiMo/ZS-3 (91.3 %) > NiMo/ZS-2 (87.6 %) > NiMo/ZS-1 (81.6 %) > NiMo/ZS-4 (76.1 %) > NiMo/ZS-5 (71.5 %) > NiMo/ZS-M (66.2 %), indicating that the NiMoS active phases increase in the same order, which is well in accordance with the Mo_{3d} XPS results of the corresponding sulfide catalysts. For the NiMo/ZS-3 catalyst, the moderate MSI, ordered pore structure and uniform morphology are expected to be responsible for the promotion of sulfidation degree, which is beneficial to the improvement of the HDS performance.

3.2.5 HRTEM of the sulfide catalysts

More information on the morphology of MoS₂ active phases formed can be investigated by the statistical results of around 400 slabs from various HRTEM images. Figures 12 (a)-(f) display the representative HRTEM images of series sulfide NiMo/ZS and NiMo/ZS-M catalysts and the corresponding stacking number distributions of MoS₂ crystallites. Figure 13 exhibits the length distribution of the MoS₂ crystallites dispersed on the series NiMo/ZS and NiMo/ZS-M sulfide catalysts. It can be observed that as the amount of ZSM-5 seeds increase in the ZS series supports, the length and stacking degree of MoS₂ slabs decrease obviously. The sulfide NiMo/ZS-1 catalyst contains a lower degree of stacking layer numbers ascribed to the strong MSI, which is restrictive to the generation of NiMoS-II active phases. Compared to NiMo/ZS-1 catalyst, NiMo/ZS-5 and NiMo/ZS-M catalysts show relatively high stacking layer numbers of MoS₂ active phases, which are restrictive to expose enough brim and edge sites for adsorption and reaction of the reactants.⁶⁰ The locations of the reactants are good for the elimination of sulfur through the perpendicular adsorption of reactants.⁶¹ NiMo/ZS-1 catalyst exhibits the appropriate stacking degree of MoS₂ phases, which can promote the generation of more NiMoS-II phases.⁵⁷ The statistical results of the average length (L_{av}), average layer number (N_{av}) and dispersion degree (f_{Mo}) of MoS₂ active phases are summarized in Table 1. The L_{av} and N_{av} values of the MoS₂ slabs over the NiMo/ZS and NiMo/ZS-M series sulfide catalysts change in the sequence of NiMo/ZS-M (5.2 nm, 3.8) > NiMo/ZS-5 (4.6 nm, 3.5) > NiMo/ZS-4 (4.3 nm, 3.1) > NiMo/ZS-3 (3.9 nm,

1
2
3 2.8) > NiMo/ZS-2 (3.4 nm, 2.5) > NiMo/ZS-1 (3.2 nm, 2.3). The f_{Mo} values of MoS₂
4
5
6 over the NiMo/ZS and NiMo/ZS-M series sulfide catalysts change in the sequence of
7
8 NiMo/ZS-1 (0.37) > NiMo/ZS-2 (0.35) > NiMo/ZS-3 (0.33) > NiMo/ZS-4 (0.29) >
9
10 NiMo/ZS-5 (0.26) > NiMo/ZS-M (0.21), which is consistent with the Raman spectra
11
12 results. NiMo/ZS-3 catalyst not only possesses the appropriate stacking degree of
13
14 MoS₂ slabs than the other five catalysts, but also possesses the relatively high MoS₂
15
16 dispersion degree, which are essential for the improvement of the HDS performance.
17
18
19
20
21
22
23
24
25
26
27
28
29
30
31
32
33
34
35
36
37
38
39
40
41
42
43
44
45
46
47
48
49
50
51
52
53
54
55
56
57
58
59
60

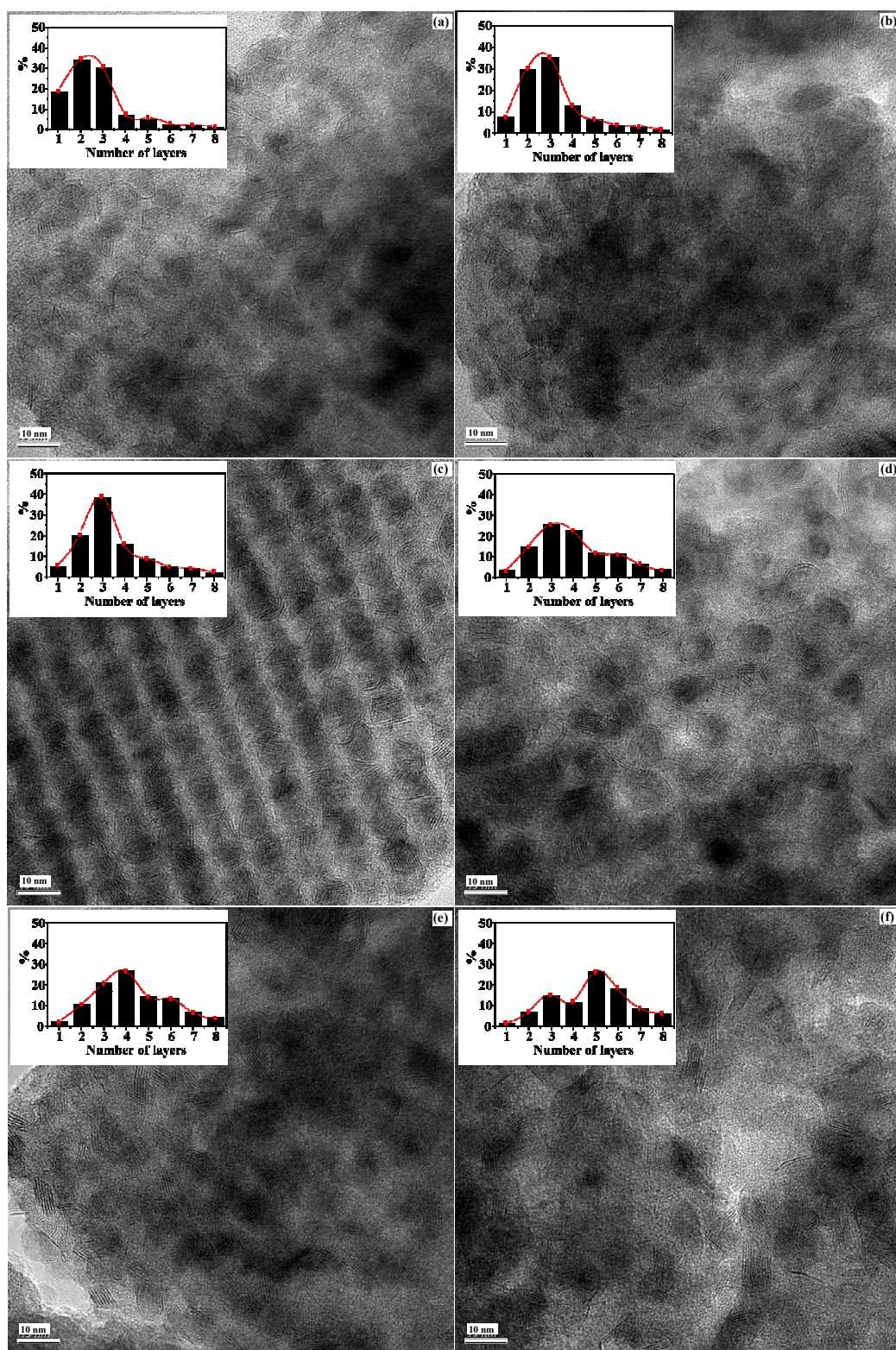


Figure 12. HRTEM images of various sulfide catalysts. (a) NiMo/ZS-1, (b) NiMo/ZS-2, (c)

NiMo/ZS-3, (d) NiMo/ZS-4, (e) NiMo/ZS-5 and (f) NiMo/ZS-M.

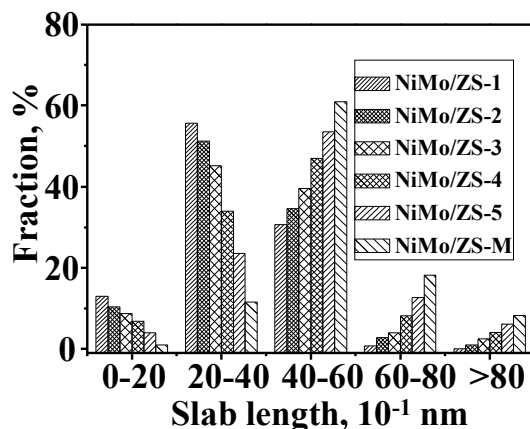


Figure 13. The length distribution of the MoS₂ slabs dispersed on various sulfide catalysts.

Table 1. *L_{av}* and *N_{av}* values of MoS₂ slabs.

Catalyst	<i>L_{av}</i> (nm)	<i>N_{av}</i>	<i>f_{Mo}</i>
NiMo/ZS-1	3.2	2.3	0.37
NiMo/ZS-2	3.4	2.5	0.35
NiMo/ZS-3	3.9	2.8	0.33
NiMo/ZS-4	4.3	3.1	0.29
NiMo/ZS-5	4.6	3.5	0.26
NiMo/ZS-M	5.2	3.8	0.21

3.3 Results of the DBT HDS

Figure 14 displayed the DBT HDS performance of series NiMo/ZS and reference catalysts at different WHSVs in the range of 10 to 100 h⁻¹. The DBT HDS activities of series catalysts increase with the decrease of WHSVs, which are derived from the extension of the contact time between reactants and catalysts. Furthermore, the DBT HDS conversions of different catalysts at all WHSVs follow the similar orders of NiMo/ZS-3 > NiMo/ZS-2 > NiMo/ZS-1 > NiMo/ZS-4 > NiMo/ZS-5 > NiMo/ZS-M > NiMo/SBA-16 > NiMo/ZSM-5. The NiMo/ZS-3 exhibits the highest DBT HDS conversions, of which its DBT HDS conversion (58.2 %) is more than two times as

that over the reference NiMo/ZS-M (25.2 %), and about three times as that over the reference NiMo/SBA-16 (20.8 %), while about four times as that over NiMo/ZSM-5 (15.4 %) at 100 h⁻¹. The highest DBT HDS efficiency can be ascribed to the synergistic effects of its ordered pore channel, uniform morphology, moderate MSI, high sulfidation degree and moderate stacking degree, which can contribute more to deep DBT HDS reaction.

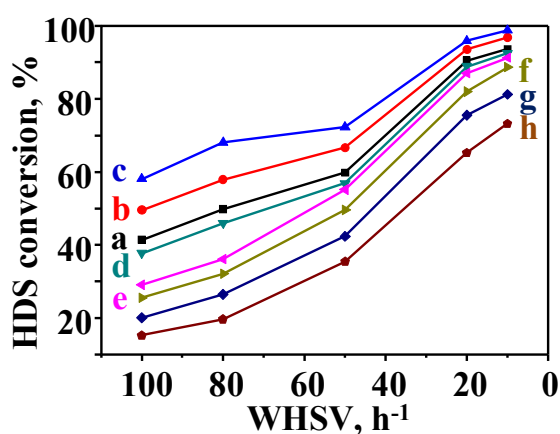


Figure 14. HDS results of DBT at different WHSVs (340 °C, 4 MPa, 200 mL/mL). (a) NiMo/ZS-1, (b) NiMo/ZS-2, (c) NiMo/ZS-3, (d) NiMo/ZS-4, (e) NiMo/ZS-5, (f) NiMo/ZS-M, (g) NiMo/SBA-16 and (h) NiMo/ZSM-5.

The product distributions (Figures S15, in Supporting Information) in the DBT HDS over NiMo/ZS-3 catalyst as a function of WHSVs are shown in Figure 15. From Figure 15, it can be found that the low WHSV can improve the DBT HDS reaction rate through direct desulfurization (DDS) other than hydrogenation (HYD), reflected from the increase of biphenyl (BP) selectivity and the decrease of cyclohexylbenzene (CHB) selectivity. DDS is the prior DBT HDS reaction route over NiMo/ZS-3,

reflected by the BP selectivity more than 50 % at different WHSVs. The selectivities of cyclopentylmethylcyclohexane (CPMCH), cyclopentylmethylbenzene (CPMB) and isophenyl hexadiene (PHDi) increase with the decreasing WHSVs, while the selectivity of tetrahydrodibenzothiophene (THDBT) decrease with the decreasing WHSVs.

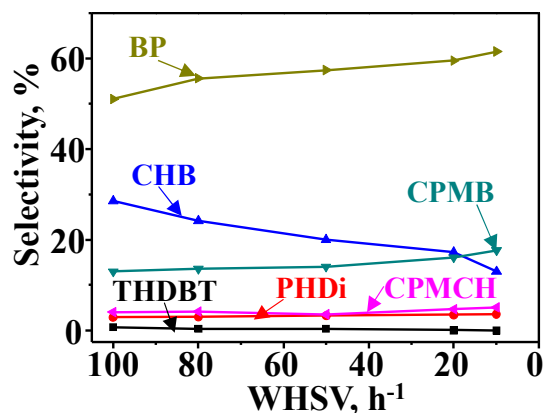


Figure 15. DBT HDS product distributions over NiMo/ZS-3 as a function of WHSVs.

In order to study the influence of morphologies of the series ZS materials on the DBT HDS reaction pathways, the products were analyzed at the similar total DBT conversion (50 %) using a GC-MS chromatograph. The DBT HDS reaction network of the series NiMo/ZS is proposed in Figure 16. Two parallel routes are found for the DBT HDS: DDS and HYD. In the DDS route, the S atom is directly removed via the breakage of C-S bonds, the characteristic of the formation of BP to be the final DDS product. In the HYD route, the hydrogenation of one aromatic ring in DBT occurs firstly, yielding THDBT intermediate. Then the intermediates are further desulfurized to generate CHEB and CHB intermediate.⁶² Furthermore, the CHB intermediate might be fully hydrogenated to dicyclohexyl (DCH). Additionally, three isomerization

products, for instance, PHDi, CPMB and CPMCH, were also detected from the DBT HDS products over series NiMo/ZS.

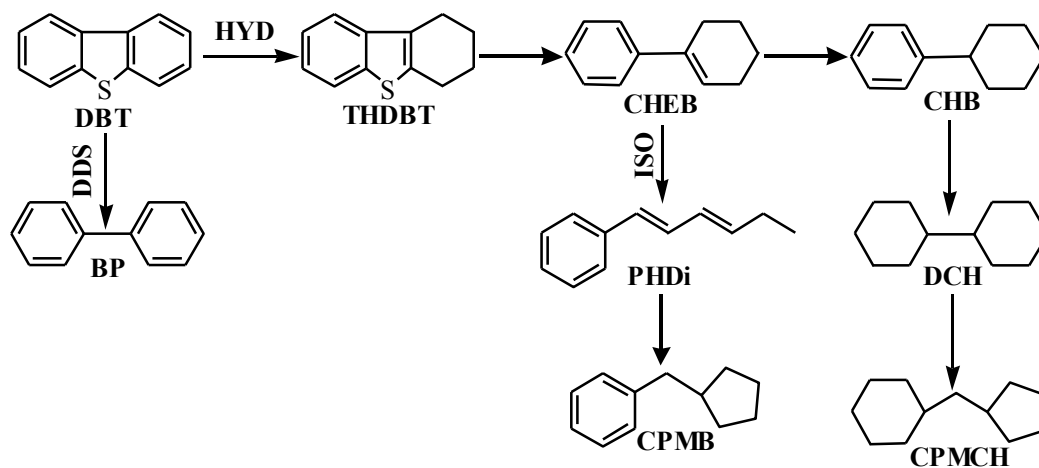


Figure 16. Possible DBT HDS reaction network of series NiMo/ZS.

The DBT HDS product distributions (Figures S14, in Supporting Information) of different catalysts are listed in Table 2. The proportions of the principal products of HYD and DDS pathways for different catalysts follow the order of NiMo/ZSM-5 (2.23) > NiMo/ZS-3 (1.22) > NiMo/ZS-2 (1.04) > NiMo/ZS-1 (0.89) > NiMo/ZS-4 (0.72) > NiMo/ZS-5 (0.64) > NiMo/ZS-M (0.54) > NiMo/SBA-16 (0.39). HYD route is the primary DBT HDS reaction pathway of NiMo/ZS-3. The high ratio of B/L acidity of NiMo/ZS-3 leads to high proportion of HYD routes, which can promote the DBT HDS performance. The k_{HDS} and TOF values of different catalysts for DBT HDS are also displayed in Table 2. The k_{HDS} and TOF values change in the sequence of NiMo/ZS-3 ($13.9 \times 10^{-4} \text{ mol g}^{-1} \text{ h}^{-1}$, 4.8 h^{-1}) > NiMo/ZS-2 ($11.0 \times 10^{-4} \text{ mol g}^{-1} \text{ h}^{-1}$, 4.1 h^{-1}) > NiMo/ZS-1 ($8.8 \times 10^{-4} \text{ mol g}^{-1} \text{ h}^{-1}$, 3.1 h^{-1}) > NiMo/ZS-4 ($6.7 \times 10^{-4} \text{ mol g}^{-1} \text{ h}^{-1}$, 3.0 h^{-1}) > NiMo/ZS-5 ($6.2 \times 10^{-4} \text{ mol g}^{-1} \text{ h}^{-1}$, 2.3 h^{-1}) > NiMo/ZS-M ($5.5 \times 10^{-4} \text{ mol g}^{-1}$

1
2
3 h^{-1} , 2.1 h^{-1}) > NiMo/SBA-16 ($4.4 \times 10^{-4} \text{ mol g}^{-1} \text{ h}^{-1}$, 1.8 h^{-1}) > NiMo/ZSM-5 (3.5×10^{-4}
4 $\text{mol g}^{-1} \text{ h}^{-1}$, 1.6 h^{-1}). The k_{HDS} of DBT over NiMo/ZS-3 is more than two times as that
5
6 over reference NiMo/ZS-M, more than three times as that over NiMo/SBA-16 catalyst
7
8
9
10 and about four times as that over NiMo/ZSM-5.
11
12
13
14
15
16
17
18
19
20
21
22
23
24
25
26
27
28
29
30
31
32
33
34
35
36
37
38
39
40
41
42
43
44
45
46
47
48
49
50
51
52
53
54
55
56
57
58
59
60

Table 2. DBT HDS performance over different catalysts.

Catalyst	Conversion ^a (%)	k_{HDS} (10^{-4} mol $g^{-1} h^{-1}$)	TOF ^b (h^{-1})	Product selectivity (%) ^c								HYD/DDS ratio
				HYD						DDS		
				THDBT	CHEB	PHDi	CHB	CPMB	CPMCH	BP		
NiMo/ZS-1	49.6	8.8	3.1	4	1	1	34	5	2	53	0.89	
NiMo/ZS-2	50.1	11.0	4.1	2	1	2	36	7	3	49	1.04	
NiMo/ZS-3	49.8	13.9	4.8	1	1	2	37	11	3	45	1.22	
NiMo/ZS-4	49.9	6.7	3.0	1	1	2	32	4	2	58	0.72	
NiMo/ZS-5	49.7	6.2	2.3	2	1	2	30	3	1	61	0.64	
NiMo/ZS-M	49.8	5.5	2.1	1	1	1	27	4	1	65	0.54	
NiMo/ZSM-5	50.2	3.5	1.6	3	1	2	42	17	4	31	2.23	
NiMo/SBA-16	50.1	4.4	1.8	1	1	1	22	2	1	72	0.39	

^a The DBT HDS conversion was obtained by changing WHSV (340 °C, 4 MPa, 200 mL/mL).

^b Number of reacted DBT molecules per hour and per Mo atom at the edge sites.

^c Determined at the total DBT conversion of 50% by changing WHSV.

HYD: THDBT + CHEB + PHDi + CHB + CPMB + CPMCH; DDS: BP.

3.4 Results of the 4,6-DMDBT HDS

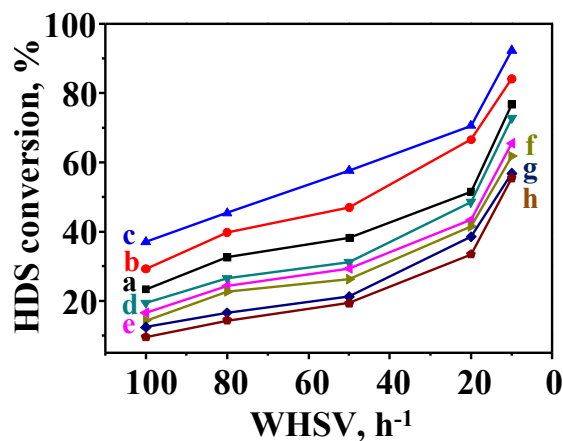


Figure 17. 4,6-DMDBT HDS results at different WHSVs (340 °C, 4 MPa, 200 mL/mL).

(a) NiMo/ZS-1, (b) NiMo/ZS-2, (c) NiMo/ZS-3, (d) NiMo/ZS-4, (e) NiMo/ZS-5, (f) NiMo/ZS-M, (g) NiMo/SBA-16 and (h) NiMo/ZSM-5.

Figure 17 displays the 4,6-DMDBT HDS performance by altering the WHSVs in the range of 10 to 100 h⁻¹. The 4,6-DMDBT HDS activities of various catalysts increase with the decrease of WHSVs. Moreover, the 4,6-DMDBT HDS performance at all WHSVs increase in the following order: NiMo/ZS-3 > NiMo/ZS-2 > NiMo/ZS-1 > NiMo/ZS-4 > NiMo/ZS-5 > NiMo/ZS-M > NiMo/SBA-16 > NiMo/ZSM-5. The NiMo/ZS-3 exhibits the highest 4,6-DMDBT HDS performance, and its 4,6-DMDBT HDS conversion (37.0 %) at 100 h⁻¹ is about three times as that over the reference NiMo/ZS-M (14.3 %), more than three times as that over the reference NiMo/SBA-16 (12.4 %), and about four times as that over NiMo/ZSM-5 (9.5 %).

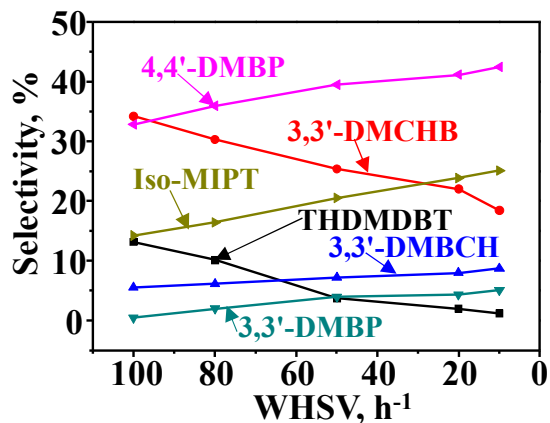


Figure 18. 4,6-DMDBT HDS product distributions on NiMo/ZS-3 catalyst as a function of WHSVs.

Figure 18 shows the 4,6-DMDBT HDS product distributions (Figures S18, in Supporting Information) of NiMo/ZS-3 as a function of WHSVs. The low WHSV can improve the 4,6-DMDBT HDS reaction rate through isomerization (ISO) routes other than via HYD, reflected from the increases of 4,4'-dimethylbiphenyl (4,4'-DMBP) and iso-methyl-isopropyltetralin (Iso-MIPT) selectivities and the decrease of tetrahydro-dimethyldibenzothiophene (THDMDBT) selectivity. DDS is not the preferential route of 4,6-DMDBT HDS over NiMo/ZS-3, reflected from the 3,3'-DMBP selectivity always less than 5.0 % at different WHSVs. The selectivity to form 3,3'-dimethylcyclohexylbenzene (3,3'-DMCHB) decreases, while the 3,3'-dimethylbicyclohexyl (3,3'-DMBCH) increases with the decreasing WHSV.

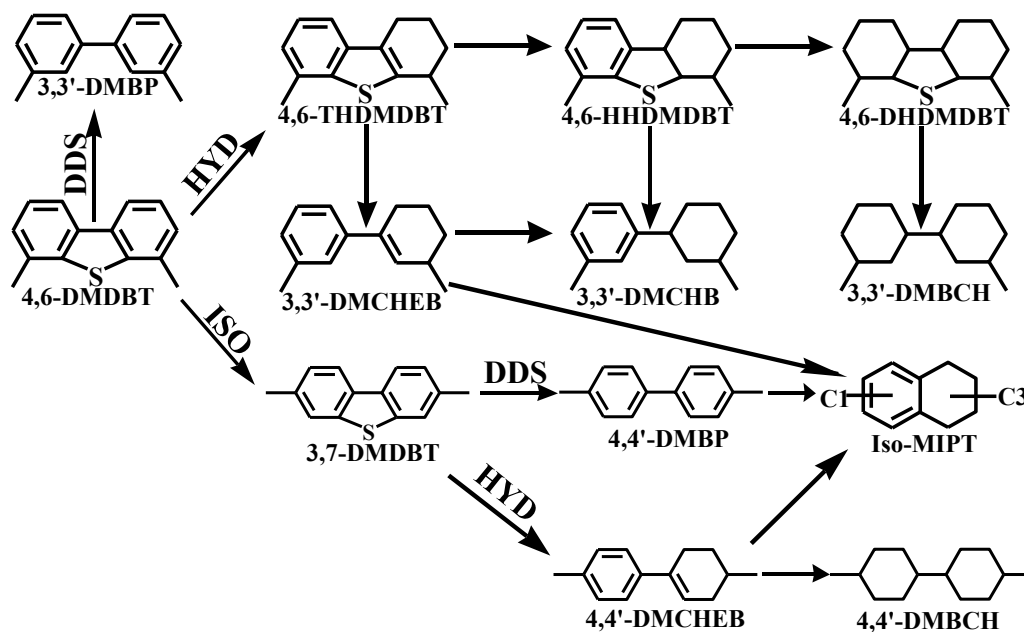


Figure 19. Possible 4,6-DMDBT HDS reaction network over NiMo/ZS catalysts.

The 4,6-DMDBT HDS products were obtained in the similar total 4,6-DMDBT conversion of 50 % using a GC-MS chromatograph (Figures S17, in Supporting Information). Figure 19 displays the 4,6-DMDBT HDS reaction network of series NiMo/ZS with different morphologies. Three parallel pathways are found for the 4,6-DMDBT HDS: DDS, HYD and ISO. For DDS, sulfur is directly removed via the breakage of C-S bonds, yielding 3,3'-DMBP. For HYD, one aromatic ring in 4,6-DMDBT is hydrogenated firstly, yielding 4,6-THDMDBT and 4,6-hexahydro-dimethyldibenzothiophene (4,6-HHDMDBT) intermediate. Then the intermediates are desulfurized to generate 3,3'-DMCHEB and 3,3'-DMCHB intermediates. Furthermore, the 3,3'-DMCHEB and 3,3'-DMCHB intermediates might be fully hydrogenated to 3,3'-DMBCH. For ISO, the migration of the methyl groups at the 4 and/or 6 positions in 4,6-DMDBT occurs firstly, yielding 3,7-DMDBT and/or

1
2
3 3,6-DMDBT intermediates. Then the sulfur is eliminated via HYD and DDS routes,
4 and DDS is the main route, yielding 4,4'-DMBP. 3,7-DMDBT and 3,6-DMDBT were
5
6 detected in 4,6-DMDBT HDS over series NiMo/ZS.
7
8
9

10 Table 3 shows the 4,6-DMDBT HDS product distributions of various catalysts.
11 The proportions of ISO for various catalysts change in the sequence of NiMo/ZSM-5
12 (63 %) > NiMo/ZS-3 (57 %) > NiMo/ZS-2 (51 %) > NiMo/ZS-1 (46 %) >
13 NiMo/ZS-4 (41 %) > NiMo/ZS-5 (33 %) > NiMo/ZS-M (29 %) > NiMo/SBA-16
14 (0 %). ISO route is the primary 4,6-DMDBT HDS reaction pathway over NiMo/ZS-3.
15
16 The high ratio of B/L acidity of the NiMo/ZS-3 leads to high proportion of ISO routes,
17 which can promote the 4,6-DMDBT DBT HDS performance. The k_{HDS} and TOF
18 values of different catalysts for 4,6-DMDBT HDS are also listed in Table 3. The k_{HDS}
19 and TOF values of 4,6-DMDBT HDS over different catalysts change in the sequence
20 of NiMo/ZS-3 (8.4×10^{-4} mol g⁻¹ h⁻¹, 2.6 h⁻¹) > NiMo/ZS-2 (6.2×10^{-4} mol g⁻¹ h⁻¹, 2.1
21 h⁻¹) > NiMo/ZS-1 (4.6×10^{-4} mol g⁻¹ h⁻¹, 1.9 h⁻¹) > NiMo/ZS-4 (3.7×10^{-4} mol g⁻¹ h⁻¹,
22 1.8 h⁻¹) > NiMo/ZS-5 (3.3×10^{-4} mol g⁻¹ h⁻¹, 1.7 h⁻¹) > NiMo/ZS-M (2.8×10^{-4} mol g⁻¹
23 h⁻¹, 1.6 h⁻¹) > NiMo/SBA-16 (1.7×10^{-4} mol g⁻¹ h⁻¹, 1.2 h⁻¹) > NiMo/ZSM-5 (1.6×10^{-4}
24 mol g⁻¹ h⁻¹, 1.1 h⁻¹). The k_{HDS} of 4,6-DMDBT over NiMo/ZS-3 is more than three
25 times as that over reference NiMo/ZS-M, more than four times as that over
26 NiMo/SBA-16 and about five times as that over NiMo/ZSM-5.
27
28
29
30
31
32
33
34
35
36
37
38
39
40
41
42
43
44
45
46
47
48
49
50
51
52
53
54
55
56
57
58
59
60

Table 3. 4,6-DMDBT HDS catalytic performance over various catalysts.

Catalyst	Conversion ^a (%)	k_{HDS} (10^{-4} mol g ⁻¹ h ⁻¹)	TOF ^b (h ⁻¹)	Product selectivity (%) ^c						Total ISO
				HYD		DDS		ISO		
				4,6-THDMDBT + 4,6-HHDMDBT	3,3'-DMCHB	3,3'-DMBCH	3,3'-DMBP	4,4'-DMBP	Iso- MIPT	
NiMo/ZS-1	50.2	4.6	1.9	6	32	9	7	31	15	46
NiMo/ZS-2	49.9	6.2	2.1	5	31	8	5	34	17	51
NiMo/ZS-3	49.8	8.4	2.6	4	29	7	3	38	19	57
NiMo/ZS-4	50.1	3.7	1.8	7	34	10	8	27	14	41
NiMo/ZS-5	50.2	3.3	1.7	9	36	12	10	23	10	33
NiMo/ZS-M	49.9	2.8	1.6	10	37	13	11	21	8	29
NiMo/ZSM-5	49.8	1.6	1.1	4	26	5	2	40	23	63
NiMo/SBA-16	50.1	1.7	1.2	14	43	17	26	0	0	0

^aThe 4,6-DMDBT HDS conversion was obtained by changing WHSV (340 °C, 4 MPa, 200 mL/mL).

^bNumber of reacted 4,6-DMDBT molecules per hour and per Mo atom at the edge sites.

^cDetermined at total 4,6-DMDBT conversion of 50% by changing WHSV.

HYD: 4,6-THDMDBT+ 3,3'-DMBCH + 3,3'-DMCHB + 4,6-THDMDBT; DDS: 3,3'-DMBP; Total ISO: Iso-MIPT + 4,4'-DMBP.

4. DISCUSSION

The DBT and 4,6-DMDBT HDS catalytic performance of various catalysts are closely connected with textural properties of the supports, MSI effect, acid properties of the catalysts, and the morphology of MoS₂ phases. Uniform morphology of the ZS series materials contributes more to the DBT and 4,6-DMDBT HDS.

The morphology of the ZS series micro-mesoporous composite materials has an important influence on the diffusion and hydrogen spillover effect. The morphology of the uniform spherical aggregates consisting of uniform hexagonal prism ZSM-5 mono-crystals can promote the shift of spillover hydrogen⁴² generated in the micropores of ZSM-5 onto nearby MoS₂ active phases in the mesopores of SBA-16, which prominently improves the HYD and ISO selectivity of the NiMo/ZS-3 catalyst. Moreover, the uniform morphology of the NiMo/ZS-3 catalyst can enhance the diffusion and accessibility between reactants and MoS₂ phases.

The pore channels of the ZS series supports have an important influence on the diffusion of DBT and 4,6-DMDBT. ZS-3 possesses the open pore channels and well-ordered arrays of cubic body-centred Im3m symmetry mesoporous structure which can provide enough space for the good diffusion property of the reactants and products.

Appropriate acid distribution and suitable B acidity of the catalysts are the significant factors for enhancing DBT and 4,6-DMDBT HDS performance.⁶³ For DBT HDS, NiMo/ZS-3 with the highest B/L ratio exhibits the highest HYD/DDS selectivity (1.22) and the highest k_{HDS} (13.9×10^{-4} mol g⁻¹ h⁻¹) and TOF (4.8 h⁻¹) values

1
2
3 of DBT HDS reaction. For 4,6-DMDBT HDS, the steric hindrances of the
4 hydrogenated intermediates of 4,6-DMDBT molecule become weaker after the shift
5
6 of the methyl groups from the 4 and 6 sites by ISO.⁶⁴ The NiMo/ZS-3 catalyst with
7
8 the highest B/L ratios shows the highest ISO selectivity (57 %), the highest k_{HDS}
9
10 (8.4×10⁻⁴ mol g⁻¹ h⁻¹) and TOF (2.6 h⁻¹) values of 4,6-DMDBT HDS reaction.
11
12
13
14

15
16 Besides, the dispersion and stacking degree of the MoS₂ active phases are closely
17 related to the MSI. Strong MSI favors the formation of the high dispersion degree and
18 low stacking degree of MoS₂ that reveal less brim and edge sites. The NiMo/ZS-3
19 catalyst possesses moderate MSI, which can promote the generation of relatively high
20 dispersion and appropriate stacking degree of NiMoS-II active phase that expose
21 more brim and edge active sites, then improving the HDS conversion. The
22 NiMo/ZS-3 catalyst shows the highest Mo_{sulfidation} (69 %) and NiMoS ratio (91.3 %)
23 and the highest DBT and 4,6-DMDBT HDS performance.
24
25
26
27
28
29
30
31
32
33
34

35 The above research findings confirm that NiMo/ZS-3 exhibits an excellent DBT
36 and 4,6-DMDBT HDS performance, which is because of its excellent textural
37 properties of the ZS-3 support, moderate MSI, the relatively high B/L ratios of the
38 catalysts, and the appropriate morphology of MoS₂ active phases.
39
40
41
42
43
44
45
46

47 **5. CONCLUSION**

48
49 Series hierarchical ZSM-5/SBA-16 composites with different morphologies were
50 prepared successfully from ZSM-5 seeds using the hydrothermal crystallization
51 method. The characterization results exhibited that ZS-3 possessed uniform
52
53
54
55
56
57
58
59
60

1
2
3 morphology and well-ordered arrays of cubic body-centred Im3m symmetry
4
5 mesoporous structure. The NiMo/ZS-3 sulfide catalyst had the relatively high
6
7 dispersion and stacking degree of MoS₂ phases which revealed more brim and edge
8
9 sites for DBT and 4,6-DMDBT HDS.
10
11

12
13 NiMo/ZS-3 exhibited the highest k_{HDS} and TOF values of DBT and 4,6-DMDBT
14
15 HDS reaction because of its synergistic effect of uniform morphology, well-ordered
16
17 pore channels, the relatively high B/L ratio, suitable MSI, appropriate dispersion and
18
19 stacking degree of the MoS₂ phases. The excellent diffusion of the uniform
20
21 morphology and high B/L ratio play a significant role on the enhanced DBT and
22
23 4,6-DMDBT HDS catalytic performance of NiMo/ZS-3.
24
25
26

27
28 The DBT and 4,6-DMDBT HDS reaction networks of series NiMo/ZS were
29
30 proposed, of which two pathways were involved for DBT HDS: HYD and DDS,
31
32 while three pathways were for 4,6-DMDBT HDS: HYD, DDS and ISO. The enhanced
33
34 B/L ratio of NiMo/ZS-3 could favor the HYD selectivity of DBT and the ISO
35
36 selectivity of 4,6-DMDBT HDS. HYD was the prior route for DBT HDS, while ISO
37
38 was the prior route for 4,6-DMDBT HDS because of high B/L ratio of NiMo/ZS-3. In
39
40 the ISO route, the shift of the methyl groups at the 4 and/or 6 sites in 4,6-DMDBT
41
42 occurs firstly over NiMo/ZS-3, the 3,7-DMDBT and/or 3,6-DMDBT intermediates
43
44 were desulfurized easily over NiMo/ZS-3. The ISO pathway significantly enhanced
45
46 the 4,6-DMDBT HDS activity of NiMo/ZS-3.
47
48
49
50
51
52
53

54 55 **ASSOCIATED CONTENT**

1
2
3
4 Supporting Information. Preparation of ZSM-5/SBA-16 composite materials (Scheme
5
6 S1), SEM images of the series ZS materials by modulating different inorganic salts
7
8 (Figure S1), SEM images of the series ZS materials by modulating different aging
9
10 temperatures (Figure S2), SEM images of the series ZS materials by modulating
11
12 different concentrations of HCl (Figure S3), Relationship between desulfurization
13
14 efficiency and particle size (Figure S4), TEM images of the series ZS and pure
15
16 SBA-16 supports (Figure S5), SEM images of pure ZSM-5 zeolite (Figure S6), ²⁷Al
17
18 NMR spectra of the series materials (Figure S7), Al 2p XPS spectra of the series
19
20 catalysts (Figure S8), HAADF-STEM and EDX elemental mapping images of ZS-3
21
22 (Figure S9), DBT HDS results at different WHSVs (Figure S10), 4,6-DMDBT HDS
23
24 results at different WHSVs (Figure S11), DBT and 4,6-DMDBT HDS results with
25
26 time on stream over NiMo/ZS-3 (Figure S12), ISO of 4,6-DMDBT to 3,7-DMDBT
27
28 over acidic catalyst (Figure S13), The DBT HDS product distributions over various
29
30 catalysts (Figure S14), The DBT HDS product distributions over NiMo/ZS-3 at
31
32 different WHSVs (Figure S15), 4,6-DMDBT HDS product distributions of
33
34 NiMo/ZS-3 (Figure S16), 4,6-DMDBT HDS product distributions of various catalysts
35
36 (Figure S17), 4,6-DMDBT HDS product distributions of NiMo/ZS-3 at different
37
38 WHSVs (Figure S18), Chemicals needed in the experiments (Table S1), Textural
39
40 properties of the series ZS supports (Table S2), B and L acid amounts obtained from
41
42 series oxide catalysts (Table S3), Mo3d XPS results obtained from series sulfide
43
44 catalysts (Table S4), and Ni2p XPS results obtained from the sulfide NiMo catalysts
45
46 (Table S5).

ACKNOWLEDGMENT

This work was supported by the National Natural Science Foundation of China (No.21676298, U1463207 and 21503152), CNOOC project (CNOOC-KJ 135 FZDXM 00 LH 003 LH-2016), the China Postdoctoral Science Foundation (Grant No. 2017M610405), the Shandong Provincial Natural Science Foundation (ZR2017BB029) and CNPC Key Research Project and KLGCP (GCP201401).

REFERENCES

- (1) Yang, R.; Hernández-Maldonado, A.; Yang, F. *Science* **2003**, 301, 79-81.
- (2) Yang, L.; Li, X.; Wang, A.; Prins, R.; Chen, Y.; Duan, X. *J. Catal.* **2015**, 330, 330-343.
- (3) Song, C.; Ma, X. *Appl. Catal. B* **2003**, 41, 207-238.
- (4) Wang, X.; Mei, J.; Zhao, Z.; Zheng, P.; Chen, Z.; Li, J.; Fan, J.; Duan, A.; Xu, C. *Ind. Eng. Chem. Res.* **2017**, 56, 10018-10027.
- (5) Lauritsen, J.; Besenbacher, F. *J. Catal.* **2015**, 328, 49-58.
- (6) Bui, N.; Geantet, C.; Berhault, G. *J. Catal.* **2015**, 330, 374-386.
- (7) Shan, S.; Yuan, P.; Han, W.; Shi, G.; Bao, X. *J. Catal.* **2015**, 330, 288-301.
- (8) Song, H.; Wang, J.; Wang, Z.; Song, H.; Li, F.; Jin, Z. *J. Catal.* **2014**, 311, 257-265.
- (9) Wang, X.; Zhao, Z.; Chen, Z.; Li, J.; Duan, A.; Xu, C.; Gao, D.; Cao, Z.; Zheng, P.; Fan, J. *Fuel Process. Technol.* **2017**, 161, 52-61.
- (10) Ho, T.; McConnachie, J. *J. Catal.* **2011**, 277, 117-122.
- (11) Wang, X.; Du, P.; Chi, K.; Duan, A.; Xu, C.; Zhao, Z.; Chen, Z.; Zhang, H. *Catal. Today* **2017**, 291, 146-152.
- (12) Liu, K.; Ng, F. *Catal. Today* **2010**, 149, 28-34.

- 1
2
3 (13) Hansen, L.; Ramasse, Q.; Kisielowski, C.; Brorson, M.; Johnson, E.; Topsøe, H.;
4 Helveg, S. *Angew. Chem. Int. Ed.* **2011**, 50, 10153-10156.
5
6 (14) Nikulshin, P.; Ishutenko, D.; Mozhaev, A.; Maslakov, K.; Pimerzin, A. *J. Catal.*
7 **2014**, 312, 152-169.
8
9 (15) Kibsgaard, J.; Lauritsen, J.; Lægsgaard, E.; Clausen, B.; Topsøe, H.; Besenbacher,
10 F. J. *Am. Chem. Soc.* **2006**, 128, 13950-13958.
11
12 (16) Sun, Y.; Wang, H.; Prins, R. *Catal. Today* **2010**, 150, 213-217.
13
14 (17) Bara, C.; Plais, L.; Larmier, K.; Devers, E.; Digne, M.; Lamic-Humblot, A.;
15 Carrier, X. *J. Am. Chem. Soc.* **2015**, 137, 15915-15928.
16
17 (18) van Haandel, L.; Bremmer, M.; Kooyman, P.; van Veen, J.; Weber, T.; Hensen, E.
18 *ACS Catal.* **2015**, 5, 7276-7287.
19
20 (19) Moliner, M.; Martínez, C.; Corma, A. *Angew. Chem. Int. Ed.* **2015**, 54,
21 3560-3579.
22
23 (20) Cabrero-Antonino, J.; Leyva-Pérez, A.; Corma, A. *Angew. Chem. Int. Ed.* **2015**,
24 127, 5750-5753.
25
26 (21) Sun, J.; Bonneau, C.; Cantin, Á.; Corma, A.; Diaz-Cabañas, M.; Moliner, M.;
27 Zhang, D.; Li, M.; Zou, X. *Nature* **2009**, 458, 1154-1157.
28
29 (22) Li, D.; Xu, H.; Guthrie, G. *J. Catal.* **2000**, 189, 281-296.
30
31 (23) Fan, Y.; Lei, D.; Shi, G.; Bao, X. *Catal. Today* **2006**, 114, 388-396.
32
33 (24) Sugioka, M.; Sado, F.; Kurosaka, T.; Wang, X. *Catal. Today* **1998**, 45, 327-334.
34
35 (25) Wu, H.; Duan, A.; Zhao, Z.; Li, T.; Prins, R.; Zhou, X. *J. Catal.* **2014**, 317,
36 303-317.
37
38 (26) de Jong, K.; Zečević, J.; Friedrich, H.; de Jongh, P.; Bulut, M.; Van Donk, S.;
39 Kenmogne, R.; Finiels, A.; Hulea, V.; Fajula, F. *Angew. Chem. Int. Ed.* **2010**, 49,
40 10074-10078.
41
42 (27) Fu, W.; Zhang, L.; Tang, T.; Ke, Q.; Wang, S.; Hu, J.; Xiao, F. *J. Am. Chem. Soc.*
43 **2011**, 133, 15346-15349.
44
45 (28) Janssen, A.; Koster, A.; de Jong, K. *Angew. Chem. Int. Ed.* **2001**, 40, 1102-1104.
46
47 (29) Kresge, C.; Leonowicz, M.; Roth, W.; Beck, J. *Nature* **1992**, 359, 710-712.
48
49 (30) Beck, J.; Vartuli, J.; Roth, W.; Leonowicz, B.; Schmidt, K.; Chu, C.; Olson, D.;

- 1
2
3 Sheppard, E.; McCullen, S.; Higgins, J.; Schlenker, J. J. *Am. Chem. Soc.* **1992**, 114,
4 10834-10843.
5
6
7 (31) Huo, Q.; Leon, R.; Petroff, P.; Stucky, G. *Science* **1995**, 268, 1324.
8
9 (32) Huo, Q.; Margolese, D.; Stucky, G. *Chem. Mater.* **1996**, 8, 1147-1160.
10
11 (33) Zhao, D.; Feng, J.; Huo, Q.; Melosh, N.; Fredrickson, G.; Chmelka, B.; Stucky, G.
12 *Science* **1998**, 279, 548-552.
13
14 (34) Valencia, D.; Klimova, T. *Appl. Catal. B* **2013**, 129, 137-145.
15
16 (35) Gao, D.; Duan, A.; Zhang, X.; Zhao, Z.; E, H.; Li, J.; Wang, H. *Appl. Catal. B*
17 **2015**, 165, 269-284.
18
19 (36) Zhang, J.; Xin, Z.; Meng, X.; Lv, Y.; Tao, M. *Fuel* **2014**, 116, 25-33.
20
21 (37) Lee, B.; Ma, Z.; Zhang, Z.; Park, C.; Dai, S. *Microporous Mesoporous Mater.*
22 **2009**, 122, 160-167.
23
24 (38) Cao, Z.; Du, P.; Duan, A.; Guo, R.; Zhao, Z.; Zhang, H.; Zheng, P.; Xu, C.; Chen,
25 *Z. Chem. Eng. Sci.* **2016**, 155, 141-152..
26
27 (39) Zhang, D.; Duan, A.; Zhao, Z.; *J. Catal.* **2010**, 274, 273-286.
28
29 (40) Simon, L.; van Ommen, J.; Jentys, A.; Lercher, J. J. *J. Catal.* **2001**, 203, 434-442.
30
31 (41) Prins, R. *Chem. Rev.* **2012**, 112, 2714-2738.
32
33 (42) Tang, T.; Zhang, L.; Fu, W.; Ma, Y.; Xu, J.; Jiang, J.; Xiao, F. *J. Am. Chem. Soc.*
34 **2013**, 135, 11437-11440.
35
36 (43) Zeng, S.; Blanchard, J.; Breysse, M.; Shi, Y.; Su, X.; Nie, H.; Li, D. *Appl. Catal.*
37 *A* **2006**, 298, 88-93.
38
39 (44) Han, Y.; Xiao, F.; Wu, S.; Sun, Y.; Meng, X.; Li, D.; Lin, S.; Deng, F.; Ai, X. *J.*
40 *Phys. Chem. B* **2001**, 105, 7963-7966.
41
42 (45) Wang, X.; Zhao, Z.; Zheng, P.; Chen, Z.; Duan, A.; Xu, C.; Jiao, J.; Zhang, H.;
43 Cao, Z.; Ge, B. *J. Catal.* **2016**, 344, 680-691.
44
45 (46) Wang, X.; Fan, J.; Zhao, Z.; Chen, Z.; Zheng, P.; Li, J.; Li, Y.; Han, L.; Duan, A.;
46 Xu, C. *Energy Fuels* **2017**, 31, 7456-7463
47
48 (47) Texier, S.; Berhault, G.; Pérot, G.; Harlé, V.; Diehl, F.; *J. Catal.* **2004**, 223
49 404-418.
50
51
52
53
54
55
56
57
58
59
60

- 1
2
3 (48) Zhang, L.; Fu, W.; Yu, Q.; Tang, T.; Zhao, Y.; Zhao, H.; Li, Y. J. *Catal.* **2016**, 338,
4 210-221.
5
6 (49) Shan, S.; Liu, H.; Yue, Y.; Shi, G.; Bao, X. J. *Catal.* **2016**, 344, 325-333.
7
8 (50) Choi, M.; Na, K.; Kim, J.; Sakamoto, Y.; Terasaki, O.; Ryoo, R. *Nature* **2009**, 461,
9 246-249.
10
11 (51) Zhao, D.; Huo, Q.; Feng, J.; Chmelka, B.; Stucky, G. J. *Am. Chem. Soc.* **1998**,
12 120, 6024-6036.
13
14 (52) Hannus, I.; Kónya, Z.; Nagy, J.; Lentz, P.; Kiricsi, I. *Appl. Catal. B* **1998**, 17,
15 157-166.
16
17 (53) Badoga, S.; Mouli, K.; Soni, K.; Dalai, A. *Appl. Catal. B* **2012**, 125, 67-84.
18
19 (54) Biswas, P.; Narayanasarma, P.; Kotikalapudi, C.; Dalai, A.; Adjaye, J. *Ind. Eng.*
20 *Chem. Res.* **2011**, 50, 7882-7895.
21
22 (55) Zhou, X.; Duan, A.; Zhao, Z.; Gong, Y.; Wu, H.; Li, J.; Wei, Y.; Jiang, G.; Liu, J.;
23 Zhang, Y. J. *Mater. Chem. A* **2014**, 2, 6823-6833.
24
25 (56) Han, W.; Yuan, P.; Fan, Y.; Shi, G.; Liu, H.; Bai, D.; Bao, X. J. *Mater. Chem.*
26 **2012**, 22, 25340-25353.
27
28 (57) Duan, A.; Li, T.; Zhao, Z.; Liu, B.; Zhou, X.; Jiang, G.; Liu, J.; Wei, Y.; Pan, H.;
29 *Appl. Catal. B* **2015**, 165, 763-773.
30
31 (58) Li, H.; Zhang, Q.; Yap, C.; Tay, B.; Edwin, T.; Olivier, A.; Baillargeat, D. *Adv.*
32 *Funct. Mater.* **2012**, 22, 1385-1390.
33
34 (59) Kibsgaard, J.; Chen, Z.; Reinecke, B.; Jaramillo, T.; *Nature Mater.* **2012**, 11,
35 963-969.
36
37 (60) Landau, M.; Vradman, L.; Herskowitz, M.; Koltypin, Y.; Gedanken, A. *J. Catal.*
38 **2001**, 201, 22-36.
39
40 (61) Gutiérrez, O.; Klimova, T. J. *Catal.* **2011**, 281, 50-62.
41
42 (62) Wang, H.; Prins, R. J. *Catal.* **2008**, 258, 153-164.
43
44
45
46
47
48
49
50
51
52
53
54
55
56
57
58
59
60

1
2
3 (63) Sun, Y.; Prins, R. *Angew. Chem. Int. Ed.* **2008**, 47, 8478-8481.
4

5 (64) Esquivel, G.; Ramírez, J.; Alejandre, A. *Catal. Today* **2009**, 148, 36-41.
6
7
8
9
10
11
12
13
14
15
16
17
18
19
20
21
22
23
24
25
26
27
28
29
30
31
32
33
34
35
36
37
38
39
40
41
42
43
44
45
46
47
48
49
50
51
52
53
54
55
56
57
58
59
60